Publications of the Astronomical Society of the Pacific

Vol. 105 **1993 March** **No. 665**

Publications of the Astronomical Society of the Pacific
105: 247–268, 1993 March

Reverberation Mapping of Active Galactic Nuclei[1]

BRADLEY M. PETERSON

Department of Astronomy, The Ohio State University, Columbus, Ohio 43210
Electronic mail: peterson@mps.ohio-state.edu

Received 1992 November 13; accepted 1992 November 19

ABSTRACT. The broad emission lines in the spectra of active galactic nuclei respond to variations in the luminosity of the central continuum source with a delay due to light-travel time effects within the emission-line region. It is therefore possible through the process of "reverberation mapping" to determine the geometry and kinematics of the emission-line region by careful monitoring of the continuum variations and the resulting emission-line response. In this review, I will discuss progress in application of the reverberation mapping technique. I will describe the underlying assumptions and limitations of the method, discuss how the results obtained to date are changing our understanding of active nuclei, and outline several new questions that might be addressed through further reverberation mapping programs.

1. INTRODUCTION

An "active galactic nucleus" (AGN) is a compact source in the center of a galaxy that emits copious amounts of radiation over a broad range of the electromagnetic spectrum. The special characteristics of AGNs, which for the purposes of this review will be restricted to type 1 Seyfert galaxies (in which the optical luminosity of the nucleus is comparable to that of the integrated starlight from the host galaxy) and quasars (in which the optical luminosity of the nucleus significantly exceeds the luminosity due to stars), have been recognized for more than 30 years. However, the nature of the "central engine" that produces the extraordinary radiated energy (in the range 10^{43-48} ergs s^{-1}) remains unknown. Excellent reviews of our current understanding of AGNs are provided by Osterbrock (1991, 1993) and by Blandford et al. (1990).

The current working model, or paradigm, for the AGN phenomenon is that the central source is a supermassive black hole with a surrounding hot accretion disk that produces the observed continuum radiation primarily via viscous heating. The basic scenario is developed from a rather straightforward interpretation of a few fundamental observations. Observations of rapid continuum variability led to the conclusion, based on coherence arguments (e.g., Terrell 1967, and references therein), that the continuum source must be very small, of order a few light days (1 lt day $\approx 2.5\times10^{15}$ cm) in some cases. The mass of this object is then suggested by the Eddington limit (Zeldovich and Novikov 1964),

$$M > 10^6 L_{44} M_\odot, \qquad (1)$$

where L_{44} is the bolometric luminosity of the AGN in units of 10^{44} ergs s^{-1}, which is characteristic of a luminous Seyfert 1 galaxy. These large masses and small radii imply a deep gravitational potential; if indeed the potential is sufficiently deep, one is led eventually to the massive black-hole scenario regardless of how one starts out arranging the material (Rees 1984).

One of the defining characteristics of Seyfert 1 galaxies and quasars is the presence in the ultraviolet and optical spectra of strong emission lines. These emission lines arise in two separate regions that are distinguished by different densities, spatial extent, and line-of-sight velocity distribution. An extended (as large as $\sim$1 kpc), low-density ($n \approx 10^3$ cm^{-3}) narrow-line region (NLR) produces emission lines with widths corresponding to line-of-sight velocity dispersions of order 500 km s^{-1}. A spatially unresolved broad-line region (BLR) gives rise to lines with widths in the range 10^{3-4} km s^{-1}. The relative strengths of the various broad lines indicate that they arise in an ionized gas at temperatures of $1\text{–}3\times10^4$ K and particle densities $n \gtrsim 10^9$ cm^{-3} (Osterbrock 1989).

The large widths of the broad lines also seem to point to a massive central source (Woltjer 1959). Thermal motions in a 10^4 K gas amount to only $\sim$10 km s^{-1}, so another broadening mechanism is required to account for the large widths of the emission lines. This is usually taken to be Doppler broadening due to bulk motions of individual gas clouds in the BLR. By assuming that the system of line-

[1]Invited review paper, based on invited presentations at the 180th Meeting of the American Astronomical Society in Columbus, Ohio, in 1992 June, and at the 33rd Herstmonceux Conference on *The Nature of Compact Objects in AGN* in Cambridge, England, in 1992 July.

emitting clouds is virialized and by estimating the size of the region from standard photoionization models (see Sec. 3.3), central masses $\sim 10^8\ M_\odot$ are inferred.

The preceding argument underscores the importance of developing an understanding of the physics of the BLR. The BLR affords a unique and important probe of the inner regions of AGNs. The dynamics of the BLR clouds are clearly determined by forces related to the central engine, namely gravitation and radiation pressure. Furthermore, the emitted line spectrum affords a diagnostic of the ionizing continuum (photon energies $h\nu > 13.6$ eV or wavelengths $\lambda < 912$ Å), which is for most practical purposes not observable in any other way, except in high-redshift sources where the continuum shape may be altered by absorption in lower-redshift gas clouds, and which in any case might not have ionizing spectra similar to those of lower-luminosity AGNs.

The physical structure of the BLR may also provide important information about the origin of this gas and about how the central engine is fueled. Studies of the extended structure of AGNs (the NLR and beyond) show that on scales of kiloparsecs, AGNs are not spherically symmetric. It is not clear, however, on what scale this asymmetry first appears: is the continuum emission from the central engine emitted anisotropically, or in fact is the asymmetry *caused* by the BLR by preferential absorption or scattering of radiation in certain directions? Thus, while the geometry of the BLR might well tell us a great deal about how the AGN phenomenon works, the physical size of the BLR projects only to several microarcseconds even in the case of the nearest AGNs, and thus conventional methods, even above the Earth's atmosphere, are incapable of providing much direct information about the BLR structure. However, as we will see below, it is possible to learn about the BLR structure in an *indirect* fashion, through study of broad emission-line variability.

One of the characteristics of the broad emission lines in AGN spectra is that they vary in flux in response to continuum variations, on time scales of days to many weeks or longer. This immediately tells us several fundamental things about the BLR:

(1) The BLR clouds are optically thick in the ionizing (Lyman) continuum, and the energy input is almost certainly via photoionization.

(2) The variability of the observable continuum in the optical ($\sim$3100–8000 Å) and satellite ultraviolet ($\sim$1000–3100 Å) is closely coupled to variability of the ionizing continuum that drives the emission lines.

(3) The rapid response of the emission lines to the continuum variations indicates that the BLR clouds must be quite close to the central source.

From these basic facts, it became clear that it is in principle possible, by detailed comparison of the continuum and emission-line variations, to determine the geometry and velocity field (i.e., velocity as a function of position) of the BLR cloud system (Bahcall et al. 1972; Fabrika 1980a,b; Blandford and McKee 1982; Capriotti et al. 1982; Antokhin and Bochkarev 1983) through what has become known as "reverberation mapping" or "echo mapping."

In this review, I will outline the basic principles involved in the reverberation mapping technique, and discuss some of the results obtained in this relatively new field as well as some of the implications of these new results. Earlier reviews on emission-line variability in AGNs include those of Peterson (1988), Netzer (1989), Penston (1991), and Peterson (1992), and these should be consulted for more complete bibliographical references to earlier work.

2. PRINCIPLES OF REVERBERATION MAPPING

2.1 Fundamentals

In order to understand how the reverberation mapping process works and to begin to develop some intuition about how various BLR geometries respond to continuum changes, we can start by considering the very simple case where the BLR clouds are distributed in a thin spherical shell of radius r which is centered on the continuum source. For the time being, assume that the clouds cover only $\sim 10\%$ of the sky as seen from the central source, and that they absorb continuum radiation from the central source which they then reemit isotropically in emission lines. Now consider how these clouds respond to an instantaneous continuum outburst (a δ-function outburst in time, like a flash bulb). The continuum pulse is then localized in a spherical shell which is expanding outward from the central source at the speed of light. After a time $t = r/c$ the continuum pulse will reach the BLR clouds, which absorb the incident radiation and reprocess it (instantaneously) into emission lines. An observer located at the continuum source will observe the emission-line response at a time $t = 2r/c$ when the return, or "echo," pulse arrives from all points on the BLR shell simultaneously.

The situation becomes somewhat more complicated for an observer away from the central continuum source, because now the observer will not be equidistant from all points on the BLR shell, and as a consequence will see different parts of the BLR respond at different times. It is useful to consider the locus of points that an observer would see responding at some time delay τ, measured relative to detection of the continuum outburst. The intersection of this "isodelay surface" and the BLR locates the individual clouds which the observer sees responding at τ. It is obvious that an isodelay surface is an ellipsoid, where the central continuum source and the observer define the two foci. In the case of AGNs, where the BLR radius is very small compared to the separation between the AGN and the observer, the isodelay surfaces are paraboloids. Figure 1 illustrates this concept, where a spherical BLR and several isodelay surfaces are shown; each isodelay surface is labeled with the light-travel time delay relative to the central source as seen by a distant observer. The most rapid response to the continuum pulse is the BLR clouds along the observer's direct line of sight to the continuum source. The largest delay is for clouds on the far side of the BLR from the observer, where a delay of $2r/c$ occurs as the outward-moving continuum pulse crosses the BLR radius and the cloud emission echo headed toward the observer retraces the same distance.

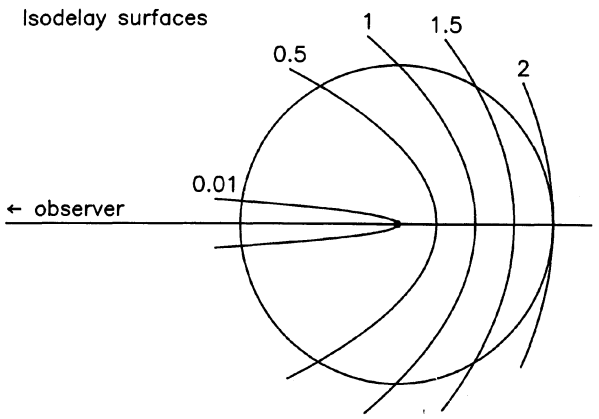

FIG. 1—Schematic view of the BLR as a thin spherical shell. The observer, to the left at infinity, sees continuum pulses propagate outward as paraboloids. At any time τ following the detection of the continuum pulse, the observer sees a response from the gas at the intersection of the BLR and an isodelay surface (with the appropriate value of τ labeled in units of r/c, where r is the BLR radius).

It is simple to compute what the total response of the BLR cloud system will look like as a function of time to an external observer. (This was first worked out for the similar case of nova shells by Coudrec 1939). At any arbitrary delay τ, the BLR clouds that will be observed to be responding to the continuum pulse are those in the locus defined by the intersection of the BLR and the appropriate isodelay surface, as shown schematically in Fig. 2. For a thin spherical shell of radius r, the intersection of these surfaces is a ring of radius $r\sin\theta$ with surface area $2\pi r^2\sin\theta\, d\theta$, where θ is the angle between the observer's line of sight and a vector from the central source to a particular point on the BLR. If we assume that the "responsivity" (which we can think of as the number of extra photons produced in a given emission line for a given increase in the continuum level) of all of the clouds is the same, the responsivity per unit area of the BLR shell ϵ is constant. The emission-line response seen by the observer is the product of ϵ and the area of the ring. The response can be written as a function of θ as

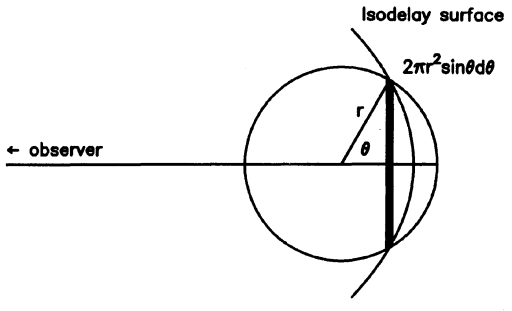

FIG. 2—The intersection between a thin spherical shell BLR and an arbitrary isodelay surface whose locus is specified by $\tau=(1+\cos\theta)r/c$. At delay τ, the observer (to the left at infinity) sees response to the continuum flux at time $\tau=0$ from clouds within the instantaneous area of intersection $2\pi r^2\sin\theta\, d\theta$.

$$\Psi(\theta)d\theta=2\pi\epsilon r^2\sin\theta\, d\theta. \tag{2}$$

The observer sees clouds at θ respond with a delay

$$\tau=(1+\cos\theta)r/c, \tag{3}$$

so the range of values of θ which correspond to fixed infinitesimal units of time is given by

$$d\tau=-(r/c)\sin\theta\, d\theta. \tag{4}$$

The line response can then be written as a function of time delay, rather than angle, as

$$\Psi(\tau)d\tau=\Psi(\theta)\left|\frac{d\theta}{d\tau}\right|d\tau=2\pi\epsilon rc\, d\tau. \tag{5}$$

We refer to $\Psi(\tau)$, which describes the emission-line response to a single continuum pulse as seen by a distant observer, as the "transfer function" for this particular geometry (see Blandford and McKee 1982). Note that in the particular case of a thin spherical shell, the transfer function is nonzero between $\tau=0$ (i.e., by Eq. [3], $\theta=180°$, corresponding to the clouds along the line of sight to the observer) and $\tau=2r/c$ (i.e., $\theta=0°$, corresponding to the far side of the BLR as seen by the observer). Moreover, it is seen that in the range $0\leqslant\tau\leqslant 2r/c$, the transfer function is *constant* (independent of τ). The simple reason for this is that while the ring which is the locus of intersection has its largest *radius* around $\theta=90°$, by Eq. (4), a fixed interval of time $d\tau$ corresponds to the smallest range in $d\theta$ at the same time; $\sin\theta$ cancels out of the equation when the transfer function is expressed in units of time delay.

Transfer functions for other possible BLR geometries, such as a disk at some arbitrary inclination, can be computed in a similar straightforward fashion. A simple case is a thick spherical geometry, which can be considered to be the superposition of several thin shells of varying radius between the inner and outer radii, $r_{\rm min}$ and $r_{\rm max}$. The transfer function for a thick spherical shell has a flat maximum in the range $0\leqslant\tau\leqslant 2r_{\rm min}/c$, and decreases monotonically to zero at $2r_{\rm max}/c$. It is important to note that much of the real physics has been put into a single term, the responsivity, which can be expected to vary with radius.

Although the reverberation mapping technique does not depend on the assumption of any particular BLR geometry, there are several fundamental assumptions which are made:

(1) It is assumed that the continuum emission originates in a single, central source that radiates isotropically and is much smaller than the BLR.

(2) It is assumed that the central source and the emission-line clouds occupy a small fraction of the total volume of the BLR and that both continuum and emission-line photons propagate freely at the speed of light within this volume.

(3) It is assumed that there is a simple, although not necessarily linear, relationship between the observable continuum and the ionizing continuum that is driving the lines.

(4) It is assumed that the light-travel time across the BLR (r/c, which is of order days to weeks) is the most important time scale.

The first of these assumptions is central to the black-hole model. We do well to keep in mind that this assumption might indeed be incorrect if multiple-source models, such as that of Terlevich (1992) and collaborators more accurately describe the central engine.

The second assumption is reasonable because the BLR "filling factor," or fraction of the total volume actually occupied by line-emitting gas, can be estimated from emissivity considerations and is found to be small (Osterbrock 1989). Also, earlier suggestions that the BLR clouds are pressure-confined by an external intracloud medium no longer seem to be viable (e.g., Mathews and Ferland 1987), so there is no evidence for an intracloud medium that might scatter or distort the wave fronts.

The third assumption cannot be tested directly. However, the close correspondence between continuum and emission-line light curves gives us some confidence that this assumption is valid at some level of approximation.

The fourth assumption requires that the cloud response to the continuum variations is nearly instantaneous. The relevant time scales to consider are the recombination time, which gives the time scale for ionization equilibrium to be established locally, and the resonance photon diffusion time, which gives the time it takes a resonance-line photon, which will undergo numerous scatterings before escaping the cloud, to travel from the ionization front to the cloud surface (i.e., through the Strömgren depth). The recombination time is given by

$$\tau_{\rm rec} \approx (n_e \alpha_{\rm B})^{-1} \approx 0.1 n_{10}^{-1} \text{ hr}, \tag{6}$$

where n_e is the electron density (n_{10} is the same quantity expressed in units of 10^{10} cm^{-3}, which is a conventional, but perhaps somewhat too small, estimate for the particle density in the BLR clouds; see Sec. 3.3) and $\alpha_{\rm B}$ is the Menzel–Baker case B recombination coefficient (Osterbrock 1989). The resonance-line diffusion time is of order 20 times the direct light-travel time through one Strömgren depth (Hummer and Kunasz 1980),

$$\tau_{\rm diff} \approx 20 \frac{R_S}{c} \approx 20 \frac{U}{n_e \alpha_{\rm B}} \approx 2 n_{10}^{-2} \text{ hr}, \tag{7}$$

where U is the ionization parameter (ratio of ionizing photons to particles at the irradiated cloud face, see Sec. 3.3).

The fourth assumption also requires that the BLR structure is constant over the duration of the reverberation monitoring experiment, i.e., at least a few times the light-travel time r/c. Assuming that the emission-line widths represent bulk motions of the clouds, the dynamical time scale for the BLR can be estimated as

$$\tau_{\rm dyn} \approx \frac{r}{v_{\rm FWHM}} \approx 2\text{–}4 \text{ yr}, \tag{8}$$

where $v_{\rm FWHM}$ is the full width at half-maximum for a broad emission line.

The numerical estimates provided here, which are based on results presented in Sec. 3, indicate that the fourth assumption is probably reasonable.

2.2 The Transfer Equation

The transfer function, introduced in Sec. 2.1, describes the response of an emission line to a δ-function continuum outburst. The actual continuum behavior of AGNs is complex, and as a result the emission-line response is the convolution of the continuum variations and the transfer function. In general, the relationship between the continuum light curve $C(t)$ and an emission-line light curve $L(t)$ is usually assumed to be described by

$$L(t) = \int_{-\infty}^{\infty} \Psi(\tau) C(t-\tau) d\tau, \tag{9}$$

which is known as the "transfer equation." The fundamental aim of reverberation mapping is to use the observables $C(t)$ and $L(t)$ to solve this integral equation for $\Psi(\tau)$ and thus infer the geometry of the BLR. In the original formulation of Blandford and McKee (1982), the transfer function is obtained by Fourier methods. In real situations, solution by Fourier transforms does not work very well since the data are rarely even close to regularly sampled, and in any case a very large number of points are required to obtain an accurate solution. In practice, a transfer function obtained by using Fourier transforms has been published for only one data set (Maoz et al. 1991). More often, the solution to $\Psi(\tau)$ is obtained by employing a maximum entropy method (MEM), as described by Horne et al. (1991), Krolik et al. (1991), and Peterson et al. (1993). A more complete description of methods for determination of the transfer function is given by Horne (1993).

Strictly speaking, Eq. (9) makes assumptions that are almost assuredly incorrect to some degree, specifically, that there is a *linear* relationship between the *observed* continuum and the emission-line fluxes. The relationship between the observed continuum and the ionizing continuum is almost certainly not so simple, and the relationship between the ionizing continuum flux and the emission-line response is also usually expected to be nonlinear, except in simple cases, such as Lyα in an optically thick, pure hydrogen nebula. However, in the MEM solutions, Eq. (9) is usually solved in a somewhat different form, with $C(t)$ written as a constant (usually the mean value) plus a time-dependent component, i.e.,

$$C(t) = \bar{C} + \Delta C(t). \tag{10}$$

The emission-line light curve is written in a similar fashion, and the problem is reduced to determination of $\bar{L}$ and solution of

$$\Delta L(t) = \int_{\tau_{\rm min}}^{\tau_{\rm max}} \Psi(\tau) \Delta C(t-\tau) d\tau, \tag{11}$$

where $\tau_{\rm max}$ and $\tau_{\rm min}$ can be selected to search for a solution in a specific range of delays (e.g., causality requires $\tau_{\rm min} \geqslant 0$, unless it is supposed that the ionizing continuum and ob-

served continuum are not in phase). This formulation not only removes the effects of constant components (such as narrow-line contributions to the emission lines and starlight to the continuum, which are absorbed in the constants $\bar{L}$ and $\bar{C}$, respectively), but is also equivalent to a first-order expansion of a nonlinear form of the transfer function. Thus, mild nonlinearity does not pose a serious problem. An important point is that in Eq. (9), the quantity that describes the emission-line physics is the "emissivity" (energy radiated in the line per unit volume of gas caused by changing the continuum level from zero to C), whereas in Eq. (11), the relevant quantity is the responsivity, or *change* in the emissivity of the line caused by changing the continuum level from $\bar{C}$ to $\bar{C}+\Delta C$.

It is important to emphasize that with limited data sets, it is generally not possible to find a unique solution for $\Psi(\tau)$ (a more complete discussion is provided by Horne 1993). It is perhaps more correct to think of MEM analysis as eliminating certain forms of $\Psi(\tau)$ and isolating others that are deemed to be more realistic on account of certain characteristics of the solution (e.g., the smoothness of the fits to the light curve or the transfer function, nonviolation of causality, etc.). It is only when there is a truly large amount of high-quality data that the possible solutions become degenerate. In cases where the data are less complete, it is possible only to exclude certain solutions as unlikely, and identify other solutions as more likely, with some weighting based on what are deemed to be the most desirable characteristics of the solution.

2.3 Cross-Correlation Analysis

Only within the last few years have AGN light curves been sufficiently well-sampled that it is possible to solve Eq. (9) directly. With less well-sampled data, it is nevertheless possible to obtain some measure of the spatial extent of the BLR by simply cross-correlating the continuum and emission-line light curves in order to find the temporal shift between them that maximizes the correlation. This shift is usually referred to as the "lag" for the particular emission line relative to the continuum. The cross-correlation function is defined as

$$F_{\mathrm{CCF}}(\tau)=\int_{-\infty}^{\infty} L(t)C(t-\tau)dt. \qquad (12)$$

The continuum autocorrelation function is defined similarly as

$$F_{\mathrm{ACF}}(\tau)=\int_{-\infty}^{\infty} C(t)C(t-\tau)dt. \qquad (13)$$

By using Eq. (9) for $L(t)$ in Eq. (12),

$$F_{\mathrm{CCF}}(\tau)=\int_{-\infty}^{\infty} C(t-\tau)\int_{-\infty}^{\infty}\Psi(\tau')C(t-\tau')d\tau'\,dt. \qquad (14)$$

By reversing the order of integration,

$$F_{\mathrm{CCF}}(\tau)=\int_{-\infty}^{\infty}\Psi(\tau')\int_{-\infty}^{\infty} C(t-\tau')C(t-\tau)dt\,d\tau', \qquad (15)$$

the interior integral is now recognized as Eq. (13) for $F_{\mathrm{ACF}}(\tau-\tau')$, so that

$$F_{\mathrm{CCF}}(\tau)=\int_{-\infty}^{\infty}\Psi(\tau')F_{\mathrm{ACF}}(\tau-\tau')d\tau' \qquad (16)$$

(Penston 1991). Thus, the cross-correlation function is the convolution of the transfer function and the continuum autocorrelation function. The lag for a particular emission line is defined to be the location of the peak (or sometimes centroid) of the cross-correlation function $F_{\mathrm{CCF}}(\tau)$. The relationship between the cross-correlation results and the transfer function is thus fairly simple in the linear-response model, although it is still clear upon some reflection that the lag measured depends not only on the transfer function, but also on the characteristics of the continuum variability, as characterized by $F_{\mathrm{ACF}}(\tau)$.

Expressed in a simple way, a cross-correlation analysis is performed by undertaking a regression analysis between the two observed light curves, $C(t)$ and $L(t+\Delta\tau)$, where $\Delta\tau$ is an arbitrary temporal shift between the two data sets. The lag is the value of $\Delta\tau$ that maximizes the correlation coefficient between the two series. In order to carry out such an analysis correctly and make use of all of the data, it is clear that the data points must be evenly spaced so that $\Delta\tau$ is some integral multiple of the sampling interval. This is a particularly difficult condition to meet with astronomical data sets on account of the observational (as opposed to experimental) nature of astronomical research. Even with space-based observations, truly regularly sampled data sets which cover a long period of time (say, several months) represent an ideal which is almost impossible to achieve.

In order to circumvent the requirement of regular sampling, various modifications have been introduced. There are two common methodologies in wide use in emission-line variability studies of AGNs. The first of these is to interpolate between real observations in the observed light curve, and resample the interpolated light curves at regular intervals (Gaskell and Sparke 1986). In order to reduce the effects of adding many interpolated points, it is preferable to interpolate in only one of the time series and perform the cross-correlation using these points and only the *real* data points from the other series; Gaskell and Peterson (1987) perform the cross-correlation twice, interpolating first in one series and then in the other, and then averaging the results. The drawback to this method is that it presupposes some understanding of the true continuum behavior on time scales shorter than are actually observed. It must be assumed that the real light-curve behavior between the observed points can be approximated by a smooth function.

A second potential problem with the interpolation method arises if there are correlated errors between the two time series. Emission-line variability studies are susceptible to such errors because it is common to measure the continuum flux and the emission-line flux from the same spectrum; any error in flux calibration scales the line and continuum fluxes by the same factor, which means that there is an artificial correlation introduced at $\Delta\tau=0$. The

interpolation process tends to compound this correlated error.

In an attempt to overcome these difficulties, Edelson and Krolik (1988) introduced the discrete correlation function (DCF) method. The basic idea behind the DCF method is to use only the observed data points in order to avoid interpolation. The cross-correlation function produced is based on all pairs of real data in the two time series that are separated by a given $\Delta\tau$. In order to increase the number of pairs which contribute to the correlation amplitude at any value of $\Delta\tau$, one can "bin" the correlation function in such a way as to include all pairs of points with separations in the range $\Delta\tau-\delta$ to $\Delta\tau+\delta$. This increases the accuracy with which the correlation amplitude is determined at $\Delta\tau$, but with some concomitant loss of temporal resolution. Moreover, one can exclude from the calculation all points where $\Delta\tau$ is identically zero (i.e., continuum and emission-line fluxes drawn from the same data) to eliminate the possibility of an artificial signal at small $\Delta\tau$ due to correlated errors.

For well-sampled time series, the interpolation method and the DCF method give results which are in good agreement (Rodríguez-Pascual et al. 1989; Peterson et al. 1991). The principal difficulty with the DCF method becomes clear, however, when the time series are less well sampled. The DCF method can easily fail to find a real correlation between two marginally sampled light curves. This is illustrated in Fig. 3, in which the results for a real AGN light curve (discussed in Sec. 3.2) are shown. In Fig. 3(a), we see that the interpolation method and the DCF method give cross-correlation functions which are in good agreement for a large data base (123 observations). However, when the light curves are reduced by arbitrarily retaining only every eighth point in the light curve, it is seen that the interpolation method still correctly locates the peak of the correlation function, but the DCF method does not find any evidence for a statistically significant correlation unless the temporal resolution is severely degraded.

Robinson and Pérez (1990) and Pérez et al. (1992a) have conducted a large number of numerical simulations and point out that there are a number of conditions under which the lags given by cross-correlation analysis are not very representative of the physical scale of the BLR. For example, in the case of a physically thick BLR (i.e., $r_{\max} \gg r_{\min}$), the cross-correlation peak will tend to occur at a lag more representative of $r_{\min}$ than the emissivity-weighted mean radius simply because smaller shells respond more coherently in time, as was previously noted by Gaskell and Sparke (1986) and Edelson and Krolik (1988). For this reason, some authors prefer to use the centroid, which is responsivity weighted, rather than the peak of the highest maximum in the cross-correlation function (Koratkar and Gaskell 1991a).

One of the most difficult and controversial questions in cross-correlation analysis is how to determine the uncertainty in the lag. This has been discussed by Gaskell and Peterson (1987), Edelson and Krolik (1988), and Maoz and Netzer (1989). While no clear consensus has emerged, the method which seems to be most widely accepted is to employ Monte Carlo simulations. This is done by assuming (a) some continuum behavior that is thought to be representative of the source and (b) a transfer function. The line response is computed from the continuum light curve and the transfer function, and then the continuum and emission-line light curve are sampled in such a way as to mimic real observations. Simulated observational errors are introduced into the data, and the fabricated data are then cross-correlated in the usual way to find the lag. This process is repeated many times to determine how much the lag can vary, depending on the transfer function, continuum behavior, sampling pattern, and error level.

2.4 Observational Constraints

The amplitude of variation for the continuum and emission-line fluxes is often not especially large. For AGNs that have been closely monitored, typical rms variations about the mean continuum value amount to 10%–30% in the optical over an observing season, with the maximum and minimum fluxes differing by less than a factor of 4–5. While the existence of variability can be detected even with data of only marginal quality, reverberation mapping requires that the uncertainties in the continuum and emission-line measurements be much smaller than the amplitude of real variation. In practice, measurements accurate to a few percent are found to give acceptable results. Obtaining data of sufficiently high quality to yield emission-line and continuum fluxes with uncertainties smaller than a few percent is every bit as important as obtaining good temporal sampling.

There are a number of systematic effects that can plague spectrophotometry of AGNs, and some of these that are particularly troublesome in variability studies have been discussed by Peterson (1988). In the following, a few special problems, and how they are currently dealt with, are noted briefly.

2.4.1 Ultraviolet Data

All of the space-based ultraviolet monitoring programs that have been undertaken have used the *International Ultraviolet Explorer (IUE)*, a joint NASA/ESA/SERC spectroscopic platform that was launched into geosynchronous orbit in 1978 January. Faint objects such as AGNs can be observed well in the low-resolution mode ($\sim$6 Å) over the range 1150–3200 Å. As *IUE* continues to function long past its 3–5 yr design lifetime, spacecraft power constraints continue to reduce somewhat the fraction of the sky that is accessible to it at any time. Despite this limitation and others imposed by its small primary mirror (45 cm) and 1970's vintage detectors, *IUE* remains one of the most productive telescopes of all time (see Kondo 1987). Its capabilities are especially well suited to spectroscopic monitoring of nearby AGNs, and it continues to be successfully employed in these programs, as well as many others.

Limitations on the quality of *IUE* spectra of AGNs are detector-related. Considerable effort has been made to get the most out of these data through careful "extraction" of the spectra from the two-dimensional format of the detec-

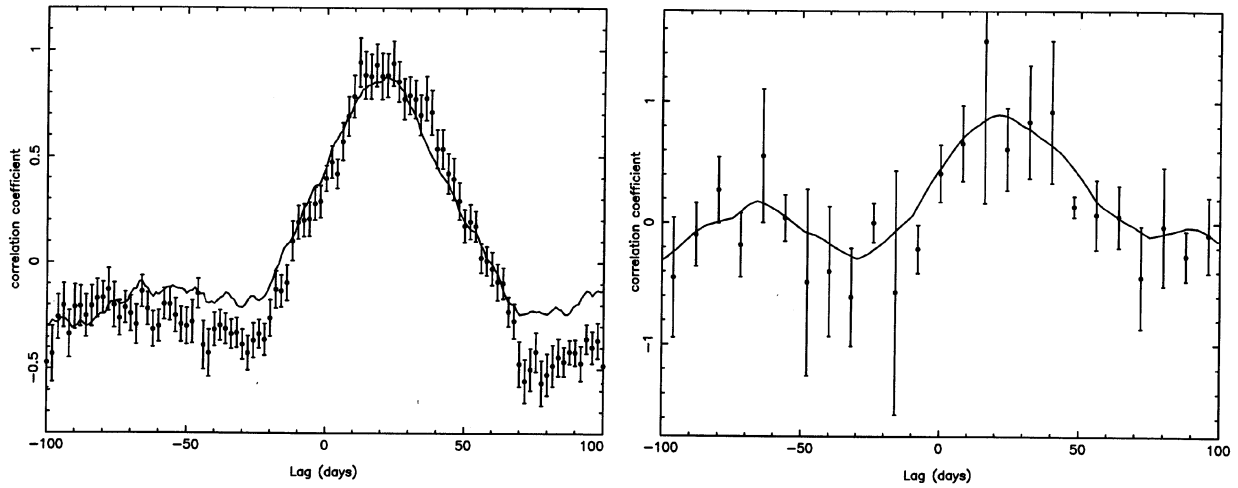

FIG. 3—Comparison of cross-correlation functions using the interpolation method and the DCF method for well-sampled and poorly sampled light curves. The cross-correlations are computed for the optical continuum and Hβ light curves from the NGC 5548 campaign of 1988–1989 (Fig. 4) between JD 2447509 and JD 2447779. The complete light curve used to compute the cross-correlations has 123 points, with an average interval between measurements of 2.2 days. (a) shows the results obtained by using the complete light curve; the cross-correlation function computed by the interpolation method is shown as a smooth line, and the DCF values are shown as individual points with associated uncertainties. The DCF values are binned at two-day intervals. (b) shows the result of reducing the sampling by arbitrarily using only every eighth point from the original light curve. The reduced sample has only 16 points, with an average interval of 17.9 days between measurements. Here the DCF values are binned at eight-day intervals. In both cases, the interpolation method yields $\tau_{\rm peak} \approx 20$ days with an amplitude $r \approx 0.9$. For the complete sample, the DCF values are in good agreement with the results of the interpolation method. However, for the reduced sample, the DCF shows only marginal evidence for a correlation between 12 and 40 days. The uncertainties in each DCF point can be decreased at the expense of temporal resolution. In order to find a correlation amplitude that is statistically significant, the DCF binning has to be increased to about 20 days. With marginally sampled data, the interpolation method is more likely to find the correct result (in this case, with an estimated uncertainty of ± 4 days, using the formula of Gaskell and Peterson 1987 for the error estimate), but the result is valid *only* if interpolation between the observations is justified.

tor. Indeed, in one case, special spectral extraction software was developed specifically to enhance the data quality for an AGN monitoring program (Reichert et al. 1991; Clavel et al. 1991). Experience has shown that continuum and emission-line fluxes (for at least the strongest lines) can be measured to an accuracy of a few percent from *IUE* data.

2.4.2 *Optical Data*

The variable transmissive properties of the Earth's atmosphere provide a challenge to ground-based monitoring programs. Absolute spectrophotometry through small spectrograph entrance apertures (projected aperture sizes smaller, and usually much smaller, than $\sim 10''$) is difficult because it requires constant atmospheric transparency and seeing and that the program object and standard star are centered identically in the aperture. Spectrophotometric accuracy better than 10%–15% is therefore rarely attained, even for point sources. The extended surface brightness distributions of AGNs exacerbate these problems. Obviously, secondary means of flux calibration are needed, in particular, methods that do not require high-transparency, or photometric, weather conditions, since such a requirement greatly limits the number of nights that can yield useful data.

A particularly robust technique is to flux-calibrate AGN spectra *internally* by assuming that the flux in the strong narrow-emission lines, such as [O III] $\lambda\lambda$4959, 5007, does not vary over the time scales of interest (many times r/c). This is a very good assumption in nearly all cases, since the narrow lines arise in an extended ($\sim 10^{2-3}$ pc), low-density ($n_e \approx 10^3$ cm^{-3}) region, so the light-travel time and recombination time [Eq. (6)] are very long (hundreds of years in each case). There are two potential difficulties with use of this method, however:

(1) The narrow-line features used for flux calibration might be difficult to isolate in some cases, and they might be blended with features which are themselves variable with time (e.g., Baribaud and Alloin 1990). An effective way to deal with this is by examining the *difference* spectrum obtained by subtracting one spectrum from another. If the spectra are not scaled correctly in relative flux, residual features appear at the location of any constant line. The relative scaling of the spectra in flux can be adjusted until the residual narrow-line features in the difference spectrum vanish. This procedure requires very high-quality data, since the signal-to-noise ratio of the difference spectrum is much lower than that of the original data. An automated scaling algorithm for AGN spectra has been developed by van Groningen and Wanders (1992), and given high-quality data, they find that it is possible to achieve relative flux calibration accuracies at the $\sim 2\%$ level.

(2) In some galaxies, the NLR is resolved spatially. In such cases the observed surface brightness distribution of the NLR on the one hand and the BLR and continuum source on the other are affected by seeing differences in quite different ways, which changes the narrow-line-based

flux calibration unless a very large aperture is used. However, it is possible to determine a correction factor for the flux calibration if the NLR surface brightness distribution is known (from narrow-band images) and the seeing is measured for each spectroscopic observation. Wanders et al. (1992) have computed seeing-dependent correction factors for the case of the Seyfert 1 galaxy NGC 3516, and these have been applied with success to small-aperture data obtained under a variety of conditions during a monitoring campaign on this source (Wanders et al. 1993).

3. RESULTS OF SPECTROSCOPIC MONITORING OF ACTIVE GALAXIES

3.1 Monitoring Programs

Numerical solutions to integral equations such as Eq. (9) require massive amounts of high-quality data. This presents a significant obstacle in reverberation mapping studies because AGNs are faint sources and, even in the case of bright, nearby Seyfert galaxies, telescopes of at least moderate aperture are required to obtain high signal-to-noise ratio data in a reasonable amount of time. Furthermore, even if a single telescope of sufficient aperture can be committed to an AGN spectroscopic monitoring program, gaps in the time series are unavoidable due to occasional unfavorable weather and equipment failures. Space-based observatories, on the other hand, obviate concerns about weather and offer the advantage of being able to observe the important ultraviolet region of the spectrum, which includes the key emission lines Ly$\alpha\lambda$1215, C IVλ1549, and C III] λ1909. However, the competition for observing time on space-based telescopes is at least as severe as it is for the largest ground-based telescopes, which makes it difficult to obtain the commitment of time necessary to carry out an AGN monitoring program.

By the late 1980's, it had become clear that efforts of unprecedented scope would need to be undertaken in order to produce data sets suitable for use in reverberation mapping. Given the likely return on the investment, however, such extraordinary programs certainly seemed to be warranted. The level of effort required would necessitate the involvement of at least several astronomers and preferably more than one telescope.

AGN spectroscopic monitoring campaigns have now been carried out successfully by several groups, notably the following (listed approximately in decreasing order of number of participants):

(1) *International AGN Watch.* This is an informal consortium of over 100 astronomers who have combined their efforts to obtain high temporal resolution, multiwavelength observations of two Seyfert galaxies, NGC 5548 (1988–present) and NGC 3783 (1991–1992). A combined *HST/IUE*/ground-based follow-up campaign on NGC 5548 is planned for 1993 (see Sec. 4.8).

(2) *LAG— "Lovers of Active Galaxies."* This is a European consortium formed to take advantage of the international time available on the La Palma telescopes, with a program of reverberation mapping one of its many goals. LAG monitored several AGNs during the first half of 1989, including NGC 3516 (Wanders et al. 1993), for which a follow-up *IUE*/ground-based campaign is planned for 1993.

(3) *EEC— "European Extragalactic Consortium."* The EEC[2] represents an ongoing effort to monitor the ultraviolet spectrum of the bright Seyfert galaxy NGC 4151 with *IUE*. The results of this 10-yr program have been summarized recently by Ulrich et al. (1991). The EEC produced some of the earliest important results in emission-line variability studies (e.g., Ulrich et al. 1984).

(4) *Wise Observatory.* In 1988, the 1.0-m telescope of the Wise Observatory in Israel was dedicated to an AGN monitoring program for six months. During this campaign, only three sources, Mrk 279, NGC 5548, and NGC 4151, varied with sufficient amplitude to carry out useful time-series analysis. This group was the first to obtain an actual transfer function from their data, for NGC 4151 (Maoz et al. 1991).

(5) *Ohio State University.* A program of spectroscopic monitoring of AGNs has been under way at Ohio State since 1982, and since 1988, spectra of several Seyfert galaxies have been taken on an approximately weekly basis. This group was the first to point out the discrepancy between emission-line response time scales and the size of the BLR predicted by the photoionization models of the time (Peterson et al. 1985).

Each of these programs has made major contributions to the field of reverberation mapping. In Sec. 3.2, attention will be focused on the ongoing International AGN Watch campaign on NGC 5548, as this program has been the most comprehensive to date and illustrates the potential of such studies.

3.2 The International AGN Watch Program on NGC 5548

Between 1988 December and 1989 August, the ultraviolet spectrum of the Seyfert 1 galaxy NGC 5548 was observed with *IUE* once every four days as part of an interagency (NASA/ESA/SERC) program, thus providing 60 observations over a 240-day period (Clavel et al. 1991). This program was complemented by a concurrent ground-based effort, which involved more than 20 telescopes and astronomers from more than a dozen countries; between 1988 December and 1989 October, 246 optical spectra, 52 photometric observations, and numerous broad-band CCD images were obtained by this consortium (Peterson et al. 1991; Dietrich et al. 1993; Romanishin et al. 1993), thus providing optical continuum, Balmer-line, and helium-line light curves during this period. Also, a light curve for the "small blue bump," a strong, broad blend of Fe II lines and Balmer continuum in the range 2000–4000 Å, has been obtained by combining the *IUE* and optical spectra (Maoz et al. 1993). The ground-based monitoring program is still continuing (Peterson et al. 1992).

Some of the light curves obtained in this study are shown in Fig. 4. The continuum behavior during the cam-

[2]Friends of the late Michael Penston will recognize his whimsical hand at work in the names of LAG and EEC.

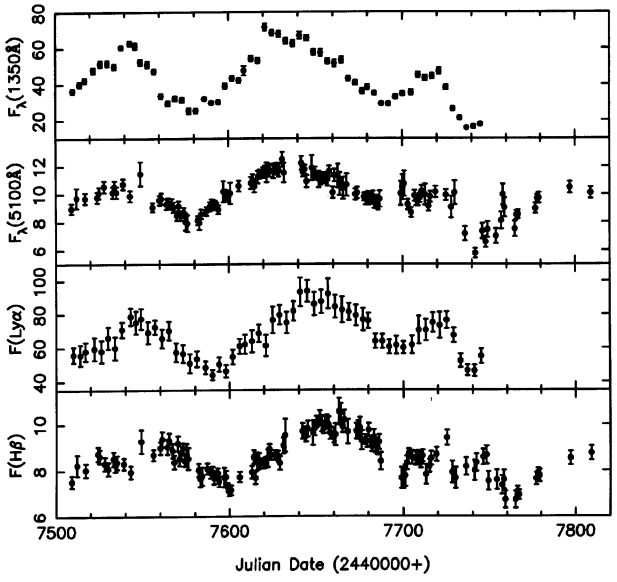

FIG. 4—Sample light curves for NGC 5548 from the 1988–1989 International AGN Watch monitoring campaign. Shown are the fluxes in the ultraviolet continuum (Clavel et al. 1991), the optical continuum (Peterson et al. 1992), the Lyα emission line (Clavel et al. 1991), and the Hβ emission line (Peterson et al. 1991). The continuum fluxes are in units of 10^{-15} ergs s^{-1} cm^{-2} Å^{-1}, and the emission-line fluxes are in units of 10^{-13} ergs s^{-1} cm^{-2}.

paign can be described in terms of three well-resolved outbursts, or "events," separated by local minima which are 50–100 days apart. The emission lines show the same pattern of variability as the continuum, although simple inspection of the light curves shows that the emission-line response is slightly delayed relative to the continuum. The delays relative to the UV continuum, determined by cross-correlation analysis as described in Sec. 2.3, are summarized in Table 1 (the value actually quoted, τ_{peak}, is the location of the peak of the cross-correlation function as computed by the interpolation method described by Gaskell and Peterson 1987). The uncertainties in the lags given in Table 1 are of order a few days in each case, except for C III] and Mg II, for which the uncertainties are considerably larger. Also shown in Table 1 are the rms variation about the mean for each line, the parameter F_{var} as defined by Clavel et al. (1991). Several important results are immediately apparent:

(1) No significant phase difference is seen between the optical and UV continuum.

(2) The UV continuum varies with greater amplitude than does the optical continuum.

(3) The delays for the various emission lines are all quite small, and show a distinct pattern of increasing lag with decreasing ionization level, thus providing clear evidence for radial ionization stratification of the BLR.

(4) The highest ionization lines vary with larger amplitude than do the lower ionization lines.

TABLE 1
NGC 5548 Cross-Correlation Results

Feature (1)	τ_{peak} (Days) (2)	F_{var} (3)
UV cont.[a]	...	0.32
optical cont.[b]	2	0.13
N V λ1240[a]	2	0.40
He II λ1640[a]	2	0.36
"Small bump"[c]	6	0.11
He II λ4686[d]	7	> 0.17
He I λ5876[d]	9	0.08
Lyα λ1215[a]	10	0.18
C IV λ1549[a]	10	0.14
Hγ λ4340[d]	13	0.11
Hα λ6563[d]	17	0.06
Hβ λ4861[b,d]	20	0.09
C III] λ1909[a]	22	0.15
Mg II λ2798[a]	34 – 72::	0.07

[a] Clavel et al. 1991
[b] Peterson et al. 1991
[c] Maoz et al. 1993
[d] Dietrich et al. 1993

The differences in the amplitude of the UV and optical continuum variations is only in part due to dilution of the optical AGN continuum by starlight; the continuum gets "harder" as the nucleus gets brighter, which seems to be a general characteristic of AGN continuum variability (Edelson et al. 1990). Parametrizing the AGN continuum as a power law in the conventional way, $F_\nu \propto \nu^{-\alpha}$, the UV/optical spectral index in NGC 5548, after removal of the starlight contribution, decreases from $\sim$0.9 in the faintest states to $\sim$0.5 in the brightest states (Wamsteker et al. 1990; Peterson 1991; Maoz et al. 1993).

The values of F_{var} for the emission lines are systematically lower than the corresponding values for the continuum. This can occur for a number of possible reasons, such as:

(1) Dilution of the amplitude of variability by the presence of constant components. Certainly, each of the broad emission lines is contaminated by a constant contribution from the NLR. However, the relative strength of the narrow-line components can be estimated fairly accurately from low-state spectra in which they appear quite clearly, and it is easy to show that these do not contribute enough flux to cause the observed low values of F_{var}. The amplitude of the line response might also be reduced if there is a nonresponsive component to the broad line which can occur, e.g., if there is an optically thin component to the emission line (e.g., Ferland et al. 1990) or if the BLR is physically extended and the outer parts of the region do not appear to respond to short time-scale continuum variations.

(2) The ionizing continuum varies with lower amplitude than does the observable continuum. The difficulties with this interpretation are (a) that this is the *opposite* from what would conclude by extrapolation of the continuum behavior from the UV/optical data, and (b) this does not explain the large amplitude variability of the highest ionization lines (N V and He II), which are driven by higher-energy photons than are Lyα and the Balmer lines.

(3) The line response to continuum variations is nonlinear. This would not be surprising for the collisionally excited lines, such as C IV and C III], but the recombination lines, Lyα in particular, are not expected to respond in a highly nonlinear way.

3.3 Implications for Photoionization Models

The particle densities in the BLR are too large to make use of the relatively simple diagnostics that can be employed to determine physical conditions in lower-density gases, such as the NLR. For this reason, we make use of more complicated photoionization equilibrium computer codes which take into account the various physical processes that operate in an astrophysical plasma, and lead to a prediction of the emergent spectrum. The general idea is to adjust the physical conditions in the model nebula to produce an emergent spectrum that matches the observed spectrum of the gas.

Photoionization equilibrium models are characterized by the shape of the ionizing continuum incident upon the gas, the chemical composition of the gas, and an ionization parameter U, which is the ratio of the ionizing photon density to particle density at the irradiated face of the cloud, i.e.,

$$U=\frac{Q(H)}{4\pi r^2 n_H c}, \tag{17}$$

where $Q(H)$ is the total rate at which hydrogen-ionizing photons are produced by the central source, r is the separation between the central source and the gas cloud (i.e., the BLR radius), and n_H is the particle density in the cloud. In the standard photoionization models of the last decade (e.g., Kwan and Krolik 1981; Ferland and Mushotzky 1982; Wills et al. 1985; Collin-Souffrin et al. 1986), the BLR is usually modeled as a single-zone ionized plasma; in other words, the emergent spectrum from a single photoionized cloud is taken to be representative of all clouds in the BLR. $Q(\mathrm{H})$ is estimated by interpolating the continuum between the observed points in the satellite ultraviolet and the X-ray region (usually 2–10 keV) in some fashion. The particle density is usually estimated as $n_H \approx 3\times 10^9$ cm^{-3}, based on the presence of broad C III] λ1909, which is collisionally suppressed at higher densities, and the absence of broad [O III] $\lambda\lambda$4959, 5007, for which the critical density is lower than 10^7 cm^{-3}. The distance r is a free parameter that essentially plays the role of a thermostat, in that the clouds can be positioned radially to control the rate of energy input by photoionization. For AGN-type spectra, a model emergent spectrum in which the line intensity ratios (the C III] λ1909/C IV λ1549 and C IV λ1549/Lyα ratios, in particular) are in reasonable agreement with observations is obtained for $U\approx 0.01$. For NGC 5548, $Q(H)\approx 10^{54}\ h_0^{-2}$ photons s^{-1} (Krolik et al. 1991; Ferland et al. 1992), where h_0 is the Hubble constant in units of 100 km s^{-1} Mpc^{-1}. We can use Eq. (17) to obtain an estimate of the BLR radius $r\approx 110 h_0^{-1}$ lt days, which is about an order of magnitude larger than the lags given in Table 1.

What went wrong in this calculation? The most important thing can be seen immediately from Table 1, namely that the assumption that C IV λ1549 and C III] λ1909 arise in the same part of the BLR seems to be incorrect. It is clear that we cannot try to model the BLR with a single representative cloud, and multiple-zone (or stratified) models will be required (e.g., Rees et al. 1989; Binette and Raga 1990; Krolik et al. 1991; Koratkar and MacAlpine 1992; Goad et al. 1993). The simple presence of C III] λ1909 is a poor density indicator; however, now there appears to be *no* clear density diagnostic, at least for the C IV/Lyα zone in NGC 5548. Indeed, the lack of significant response of C III] at $\tau\approx 10$ days (discussed further in Sec. 3.4) would seem to provide only a *lower limit* of $\sim 10^{10}$ cm^{-3} for this region, not an upper limit as previously supposed.

More recent models of the C IV/Lyα zone suggest that densities of $\sim 10^{11}$ cm^{-3} are probably appropriate for this region (Ferland et al. 1992). At higher densities, lines which are normally weak in AGN spectra, such as C III λ977 and Al III λ1860, start to become too strong in the models as the lines which are normally strongest thermalize and more of the energy must be carried away by other, normally weaker, lines. At lower densities, one would still expect C III] λ1909 to respond to continuum variations. It is worth noting additionally that 10^{11} cm^{-3} is the lowest particle density where gas pressure dominates over radiation pressure; the clouds are not stable against disruption by radiation pressure at lower densities.

With an adopted density of $\sim 10^{11}$ cm^{-3}, $Q(H)$ as given above for NGC 5548, and $r\approx 10$ lt days, the ionization parameter is $U\approx 0.04 h_0^{-2}$, only somewhat higher than used previously.

One of the interesting consequences of these new parameters is that the clouds are very optically thick in most of the important emission lines, and the line emission escapes from the clouds primarily through the side of the cloud which is irradiated by the continuum source (Ferland et al. 1992). For parameters thought to characterize the C IV/Lyα zone, nearly all of the Lyα emission is emitted through the irradiated face. For C IV and Hβ, the fraction of line emission emerging from the irradiated face is about 70% and 80%, respectively. It has been known for over a decade that Lyα emission from the clouds should be emitted in such an anisotropic fashion (Ferland and Netzer 1979; Ferland et al. 1979), and it was not understood why the Lyα emission-line profiles are, at least to first order, similar to the other broad line profiles. The fact that *all* of the strong lines seem to be emitted anisotropically appears to solve this conundrum.

3.4 Transfer Functions for the AGN Watch Data

The NGC 5548 light curves obtained by the AGN Watch are sufficiently well-sampled that it is possible to go beyond the cross-correlation analysis described in Sec. 3.2 and solve directly for the transfer function [Eq. (9)]. This has been done by Horne and his collaborators for both the UV data (Krolik et al. 1991) and the optical data (Horne et al. 1991) by employing the MEM techniques described briefly in Sec. 2.2. Some of the results of this analysis are shown in Fig. 5, which shows updated versions of these transfer functions, kindly provided by Keith Horne. It should be noted first of all that several of the transfer functions for individual lines seem to have secondary peaks well

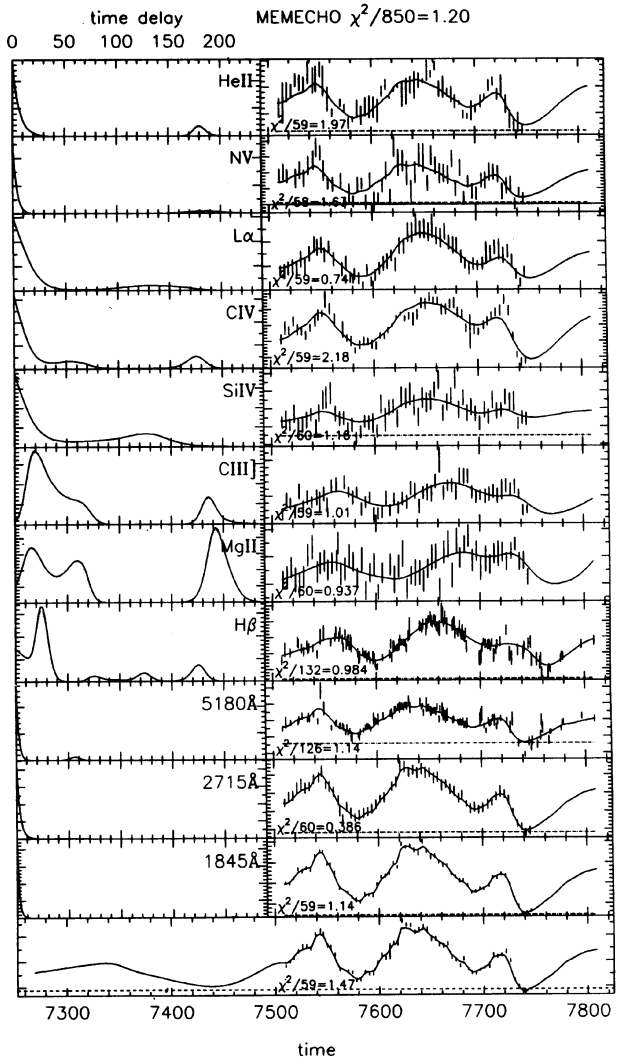

FIG. 5—Sample transfer functions for NGC 5548 during the 1988–1989 campaign. The transfer functions are shown along the left-hand side. The lower panel shows the ultraviolet continuum at 1350 Å, and the adopted fit to the light curve. The right-hand side shows the observed response and the fit to it; the fit is the convolution of the 1350 Å light curve and the transfer function. The dashed lines show the adopted background levels. Transfer functions are shown for He II λ1640, N V λ1240, Lyα, C IV λ1549, Si IV λ1400, C III] λ1909, Mg II λ2798, and Hβ. Transfer functions for other continuum bands (at 5180, 2715, and 1845 Å) are also shown to emphasize the near simultaneity of the continuum variations through the UV and optical. Figure courtesy of Keith Horne.

displaced from zero delay. These secondary peaks are thought to be due to aliasing that occurs because of the quasiperiodic nature of the three continuum events that occurred during the campaign. The noteworthy characteristics of these transfer functions are:

(1) All of the transfer functions are relatively narrow, which indicates that in each case the line response is confined to a fairly narrow range in radius. The MEM formalism seeks a smooth solution for the transfer function, so the real transfer functions may be even narrower than those shown in the figure.

(2) The transfer functions whose peaks are well displaced from zero delay (i.e., C III], Mg II, and Hβ) show a deficit of response (relative to a spherical shell) at zero delay. The real transfer functions of the other lines may have similar behavior, but because of the combination of rapid response and limited temporal resolution, a real decrease in the amplitude of the transfer function at zero delay probably would not be resolved with the present data.

Despite the narrowness of the transfer functions, there is still evidence that a thick geometry may be appropriate, for at least some of the lines— indeed, it would be unthinkable to suppose that Lyα and the Balmer lines arise in completely different regions rather than having overlapping responsivity distributions that peak at different distances from the central source. Netzer and Maoz (1990) have performed the cross-correlation analysis separately for each of the three events observed during the 1988–1989 observing season, and find that the lag for Lyα is different for each of the events, ranging from 3 days for the third and weakest event to 16 days for the second and strongest event. This pattern holds for all of the lines where the event is well resolved. For a shorter monitoring period in 1990, Clavel et al. (1992) found all of the lags were shorter than those given in Table 1 by about a factor of 3. It is important to emphasize that this does *not* necessarily require that the central source assumption (Sec. 2.1) is incorrect, nor does it require that the transfer function change on short time scales; from Eq. (16), it is clear that different continuum behavior can easily lead to differences in the lags measured, particularly if the transfer function is not narrow and has some structure. For example, Netzer (1991) has constructed a heuristic model of a thick Lyα region with $r_{\min}=2$ lt days and $r_{\max}=60$ lt days which gives the right lag for each event; while this simple model matches the light curve phases well, the amplitudes of the various events are poorly modeled if the line response is linear. We will return to this point in Sec 3.5. Netzer and Maoz (1990) have also suggested that a thick BLR geometry can explain the very different optical continuum-Hβ lag measurements obtained by the AGN Watch in 1989–1990 (21 days; Peterson et al. 1991) and by the Wise Observatory program in 1988 (7 days; Netzer et al. 1990).

If it is indeed true that at least some of the transfer functions peak away from zero delay, the simple isotropically emitting spherical shell model discussed in Sec. 2.1 is untenable. A low amplitude at zero delay means that we are not observing any emission-line response due to gas along our line of sight to the continuum source. This might indicate an absence of gas between us and the continuum source, which would occur if the BLR is in a more or less flattened configuration seen along its axis (a face-on disk). The problem with this interpretation is that it then becomes hard to explain the large widths of the broad emission lines, which presumably reflect the line-of-sight velocity distribution—either a disk would have to have physically untenable axial velocities to account for the large linewidths, or some non-Doppler broadening mechanism, such as electron scattering, is operating (indeed,

electron scattering is important in the models of Ferland et al. 1992 and Emmering et al. 1992). Another possibility is that the line emission from the BLR clouds is radiated anisotropically, as discussed in Sec. 3.3. Ferland et al. (1992) show that the Hβ transfer function is consistent with even a spherical distribution of clouds which radiate anisotropically. It should be pointed out that there is still some question about whether or not the deficit of response at small lags is real (Maoz 1992), since it is possible to find MEM solutions which do not require this (see also Peterson et al. 1993 and Horne 1993) and there may be other forms of the responsivity that have not yet been investigated (Sec. 4.6).

It is impossible at this point to consider how general any particular form of the transfer function might be. Other than those obtained from NGC 5548, the only other published transfer functions are for Hβ in Mrk 590 (Peterson et al. 1993), which also shows a deficit of response at small delays, and for Hα in NGC 4151 (Maoz et al. 1991), which is peaked at zero and consistent with a spherical, isotropically emitting distribution. Additional transfer functions are expected to become available in the near future through the AGN Watch, LAG, Ohio State, and other monitoring efforts.

The question of whether or not transfer functions in general have a relatively small amplitude at small delay is fundamentally important. It is usually assumed that the BLR gas is in some way related to how the central engine is fueled. Accreted gas from farther out in the galaxy will naturally settle into a flattened configuration unless it has zero net angular momentum, which is exceedingly unlikely. In this scenario, a flattened disk configuration is expected for the BLR. On the other hand, there have been suggestions in the literature that the BLR gas is either material ablated off stars as they pass close to the central source[3] or the extended atmospheres of stars that are heated by the AGN (Voit and Shull 1988; Scoville and Norman 1988; Penston 1988; Kazanas 1989; Schaaf and Schmutzler 1992). Stars, unlike gas, will not lose angular momentum via dissipative processes, and we would expect stars in the BLR to be more or less spherically distributed. Thus, depending on the origin of the BLR gas, two very different types of BLR geometry might be expected, and it is thus of keen interest to try to distinguish between these two possibilities. Unfortunately, we see that the likelihood of anisotropic line emission makes it impossible to distinguish between a face-on disk and a spherical distribution on the basis of the transfer function alone; we will return to this issue and how it might be resolved in Sec. 4.4

3.5 Diagnostics of the Continuum

That analysis of nebular spectra can be used to discern some of the characteristics of the unobservable ionizing continuum has long been known to astronomers, and is in fact the premise behind measurement of Zanstra temperatures of the ionizing stars in Galactic nebulae (Osterbrock 1989). In the case of AGNs, we can learn something about the shape of the ionizing continuum by examining the response of lines which respond primarily to different regions of the spectrum; e.g., Lyα is most sensitive to the continuum just shortward of 912 Å (i.e., $h\nu \geqslant 13.6$ eV), whereas the He II variations are driven by the continuum at wavelengths shorter than 228 Å (i.e., $h\nu \geqslant 54.4$ eV).

TABLE 2
NGC 5548 Integrated Line Response for Events

Event (1)	Dates (JD) (2)	Lags Lyα (days) (3)	Lags C IV (days) (4)	Log Integrated Energy Continuum (1350 Å) (ergs Å^{-1}) (5)	Log Integrated Energy Lines Lyα (ergs) (6)	Log Integrated Energy Lines C IV (ergs) (7)	Integrated Equivalent Width (Å) Lyα (8)	Integrated Equivalent Width (Å) C IV (9)
1	2447510 – 2447577	11	10	46.43	48.38	48.49	88	90
2	2447581 – 2447692	17	22	46.81	48.65	48.67	69	72
3	2447696 – 2447745	2	5	46.24	48.09	48.32	72	120

In Sec. 3.4, it was noted that the different lags for the different events can be reproduced with a thick geometry. It is easy to see how the apparent line response will be different for a very narrow (in time) continuum pulse, which illuminates only a very small part of the BLR at any one time, than for a broad continuum pulse, which can illuminate the entire BLR at once. However, if the pulse width is the only variable in a linear-response model, then the ratio of the total continuum energy in the pulse to the total line energy produced by the pulse should be the same for all events, regardless of the shape of the pulse. We can test this by integrating the energy in each of the three events observed during the NGC 5548 campaign for both the lines and continuum. The results of this experiment are summarized in Table 2. The integrated energy in each event was approximated by integrating the light curves above a linear background light curve interpolated between the local minima between events. Column (2) of Table 2 give the event boundaries for the continuum (see Fig. 4) integration. The lags ($\tau_{\rm peak}$) for Lyα and C IV λ1549 are given for each event in columns (3) and (4), respectively. The total energy (for $h_0 = 1$) in each event is given for the UV continuum at 1350 Å in column (5), for Lyα in column (6), and for C IV in column (7). Column (8) gives the ratio of Lyα energy to UV continuum energy for the entire event, which is essentially an "integrated equivalent width" (in units of Angstroms) for the event, and the same measure for C IV appears in column (9). It should be noted that these measures are highly uncertain because they are very sensitive to placement of the constant, or at least slowly varying, background component. The integrated equivalent widths in the last two columns are the most revealing: the Lyα equivalent width does not vary much between events, but the C IV response is markedly different for the third event than for the other two. In other words, the third event produced much more C IV per unit continuum energy, or per unit Lyα energy. This probably

[3]It is worth noting that stars within the BLR will not be disrupted by the intense radiation field. As Blandford (1992) has pointed out, the equilibrium blackbody temperature at 10 lt days from the central source in NGC 5548 is only $T \approx 2000$ K, and a stellar atmosphere can easily deal with this extra energy.

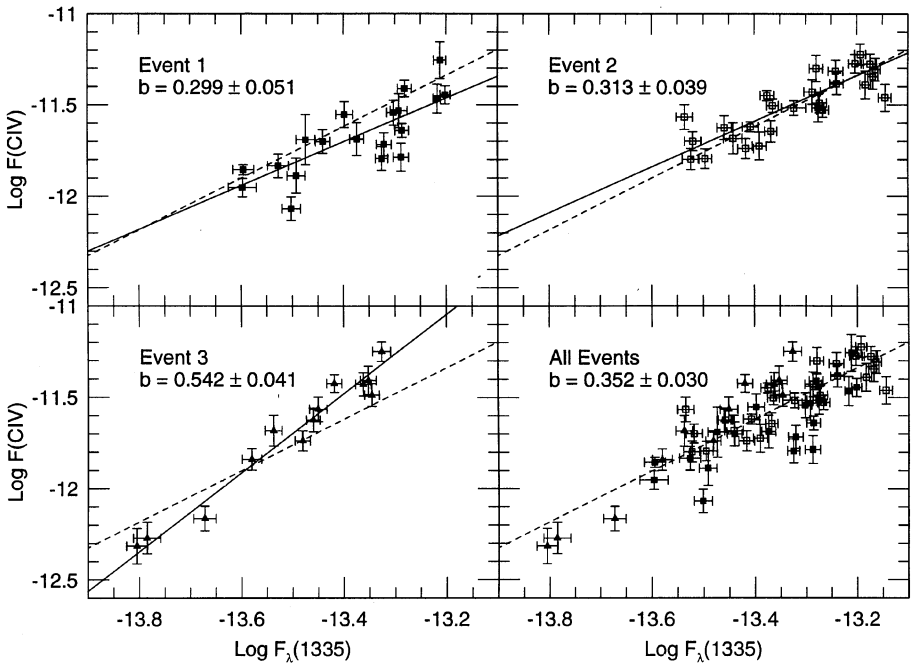

FIG. 6—The relationship between the C IV λ1549 flux, measured at time t, and the 1335 Å continuum flux at time $t-\tau_{\rm peak}$, for each of the three events observed in NGC 5548 during the 1988–1989 campaign. The data have been fitted with a relationship $\log F(\text{C IV}) \propto b \log F_\lambda(1335\ \text{Å})$, with b as given in the figure. The dashed line shows the best fit to all the data, as in the lower right panel. The best fits for each of the three events are shown separately as a solid line in the other panels. Note that, as described in the text, the slope is much steeper for the third event. The continuum fluxes F_λ(1335 Å) are in units of ergs s^{-1} cm^{-2} Å^{-1}, and the emission-line fluxes F(C IV) are in units of ergs s^{-1} cm^{-2}. Figure courtesy of Richard W. Pogge.

indicates that the ionizing continuum was considerably harder during the third event. This greatly complicates reverberation mapping, because it is clear that one cannot discern the detailed continuum behavior from a measurement at a single wavelength.

Another way to look at this is to plot the emission-line flux as a function of the continuum flux. This relationship is usually parametrized as

$$L_{\rm line} \propto L_{\rm cont}^{\lambda}. \qquad (18)$$

A relationship of this form, with $\gamma \lesssim 1$, applies to AGNs in general, i.e., from object to object, and this is known as the "Baldwin Effect" (e.g., Baldwin 1977; Kinney et al. 1990, and references therein). However, as shown by Kinney et al. (1990), a relationship like Eq. (18) also applies to individual objects as they vary in continuum luminosity. This "intrinsic" relationship is characterized by smaller values of γ than the global, or object-to-object, relationship. Because of the light-travel time delay between the continuum and line variations, the proper way to examine the intrinsic Baldwin relationship is to compare the emission-line flux at a time t to the continuum flux at time $t-\tau$, where τ is the lag for the line, since this references the line flux to the continuum which is driving it (Krolik et al. 1991; Pogge and Peterson 1992). Pogge and Peterson (1992) have done this for C IV and Lyα, and find that accounting for light-travel effects in this way removes virtually all of the random scatter in this relationship for Lyα, and removes much of the scatter in the C IV relationship; much of the remaining scatter in the C IV relationship appears to be attributable to a different slope for the third event, as shown in Fig. 6. The steeper slope of the C IV–continuum relationship for the third event also points to greater C IV production per unit continuum in the third event.

An additional indicator of the shape of the ionizing continuum is provided by the behavior of the C IV/Lyα flux ratio as a function of the continuum flux. A characteristic of all standard photoionization models is that this ratio should increase with the continuum. In Fig. 7 this ratio is shown as a function of the UV continuum flux for the first two events; each C IV/Lyα ratio is referred to the continuum eight days earlier to reduce light-travel time effects. The behavior of this ratio is exactly the opposite of the usual prediction, as this ratio is observed to *decrease* as the continuum flux increases. This behavior is also seen in other sources, notably Fairall 9 (Binette et al. 1989; Clavel and Santos-Lleó 1990) and 3C 120 (Gondhalekar 1992), and has been interpreted as an indication that the ultraviolet continuum does not continue to rise with photon energy, but rolls over at energies lower than 20 eV.[4] Zheng (1991) shows that for AGNs in general the C IV/Lyα ratio and C IV equivalent width are anticorrelated with the relative strength of the "big blue bump," which is often identified as thermal emission from the accretion disk (e.g.,

[4]We note in passing, however, that the C IV/Lyα flux ratio does indeed increase with the continuum during the third event, consistent with the earlier discussion.

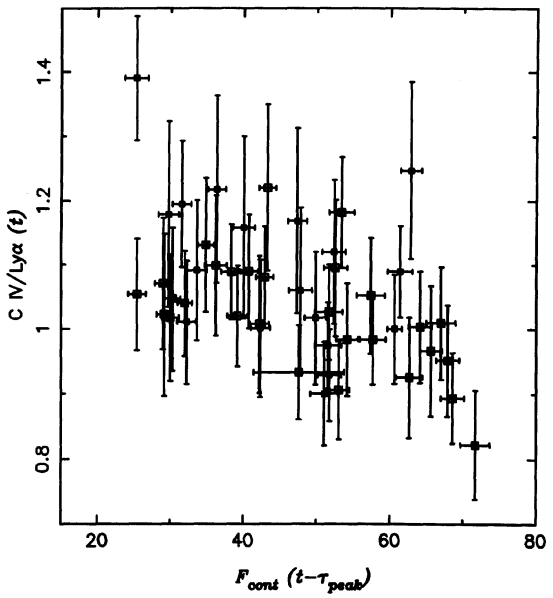

FIG. 7—The C IV/Lyα flux ratio at time t as a function of the ultraviolet continuum flux F_{cont} at time $t-\tau_{peak}$ for the first two events during the 1988–1989 NGC 5548 campaign. Contrary to the predictions of most photoionization models, this flux ratio *decreases* as the continuum flux increases. The continuum fluxes are in units of 10^{-15} ergs s^{-1} cm^{-2} Å^{-1}.

Malkan and Sargent 1982), and this suggests that the roll-over in the extreme ultraviolet spectrum is a general characteristic of AGNs.

4. UNRESOLVED AND NEW QUESTIONS

The results described in Sec. 3 represent a great step forward in our understanding of the central environs of AGNs. However, as is the nature of exploratory programs, rather than provide us with complete answers, it has led us to ask more sophisticated questions. While some of these questions can be addressed with the existing data, in many cases further data will be required, either of higher quality, higher temporal resolution, higher spectral resolution, or broader wavelength coverage. In this section, I will outline what I believe are some of the key questions that can be addressed by reverberation mapping, and discuss briefly some programs that are being undertaken toward their solution.

4.1 The Nature of the UV/Optical Continuum and Relationship to the X-ray Continuum

To theorists who are trying to explain the origin of AGN continuum radiation, perhaps the most profound result of the AGN Watch program on NGC 5548 is that the UV and optical continua vary virtually in phase, with the optical lagging behind the UV by 2 ± 2 days. A similar constraint has been obtained for NGC 4151 (Clavel et al. 1990). This result severely strains standard thin accretion-disk models (e.g., Shakura and Sunyaev, 1973; Lynden-Bell and Pringle 1974; Laor and Netzer 1989), because the UV and optical continua are expected to arise in different parts of the disk, and disturbances that produce continuum variability are expected to propagate through the disk at the sound speed. The absence of a detectable phase difference between the UV and optical continuum variations implies that a very rapid signal, with a radial velocity of order $\sim 0.1c$, coordinates the different radiating regions (Courvoisier and Clavel 1991; Collin-Souffrin 1991; Krolik et al. 1991; Molendi et al. 1991).

As an alternative to the thin-disk model, it has been suggested that the observed UV and optical radiation is due to reprocessing of higher-energy radiation (Collin-Souffrin 1991; Rokaki and Magnan 1992; Clavel et al. 1992), although it has also been argued that the reprocessing occurs in the other direction, with the X rays produced by Comptonization of the extreme ultraviolet continuum (e.g., Courvoisier 1991). There are two principal lines of evidence that argue for reprocessing of the X rays into lower-energy photons. First, the X-ray spectrum of NGC 5548 is best explained with such a model (Nandra et al. 1991). The "soft excess," or rise in the continuum at the low-energy end of the X-ray band (less than ~ 2 keV), the "hard tail" (10–20 keV), and Fe$K\alpha$ emission line (at ~ 6.4 keV) can all be explained by a power-law source of X rays illuminating an optically thick gas (perhaps the accretion disk); the emission lines and soft excess arise from absorption and reemission of the primary X rays, and the hard tail is due to Compton reflection (Nandra et al. 1991, and references therein). The reprocessing region must be quite close to the primary source because of the small time lag (a few hours) between variations of the incident power-law continuum and the hard tail (first noted by Kaastra and Barr 1989). Second, the characteristics of X-ray continuum variability suggest that reprocessing is occurring. The X-ray flux is correlated with the UV flux in NGC 5548 (Clavel et al. 1992), but with considerable scatter. This has also been noted in other sources (e.g., Morini et al. 1986; Perola et al. 1986; Maraschi et al. 1991). The X-ray continuum shows rapid variability on time scales of hours or less (Nandra et al. 1991), also characteristic of AGNs in general (see McHardy 1988), but such variations are not detected in the UV/optical (Walter and Courvoisier 1991). This has also been noted in the case of NGC 4051, where rapid X-ray variability is not accompanied by similar variations in the optical (Done et al. 1990). The difference in temporal behavior between the X-ray and lower-energy continuum is also reflected in the shape of the variability power spectrum, which is described approximately by $P(f) \propto f^{-(2-3)}$ for the UV continuum over the range of frequencies covered by the 1988–1989 campaign (Krolik et al. 1991), and in general X-ray spectra show relatively more variability at high frequencies, with $P(f) \propto f^{-(1-2)}$ at higher energies (McHardy 1988). These characteristics can be understood at least qualitatively if the X-ray region represents the primary emission and the lower-energy continuum represents reprocessing of this energy.

The relationship between the UV/optical continuum and the X-ray continuum is poorly understood. Clearly what is needed is extended simultaneous monitoring in

both parts of the spectrum for an extended period. If the UV/optical continuum is a reprocessed version of the X-ray continuum, it might be possible to describe their relationship in terms of a simple expression like Eq. (9).

4.2 The Relationship Between UV/Optical and IR Continua

Reprocessing also appears to be important in explaining the origin of the near-infrared continuum. In this case, the reprocessing agent is dust. It was first shown in the case of Fairall 9 (Clavel et al. 1989) that the 2.1 μm continuum shows the same variations as seen in the UV/optical, but with a time delay of around 400 days. Since graphite grains at a distance of 400 lt days from the central source will have a temperature close to their sublimation temperature ($\sim$1500 K; Barvainis 1987), the interpretation of this emission as arising in dust is given considerable credence. Similar lags between the UV/optical and near-IR continua also have been detected in GQ Comae (Sitko 1991), NGC 3783 (Glass 1992), and NGC 1566 (Baribaud et al. 1992).

Barvainis (1987) and Sanders et al. (1989) independently suggested that the near-IR continuum in AGNs is due to hot dust in the vicinity of the central source in order to explain the ubiquitous local depression in AGN spectra at $\sim$1 μm. The reemitted spectrum from hot dust disappears at wavelengths shorter than $\sim$1 μm because dust does not exist at higher temperatures.

Further coordinated UV/optical/IR observations of additional sources should reveal whether or not it is generally true that the near-IR continuum is due to reprocessing by dust, rather than an extension of the X-ray power-law continuum (e.g., Elvis et al. 1986). Rapid IR continuum variations, which might be expected if the IR continuum is an extension of the X-ray continuum, have been searched for but not found in the rapidly varying X-ray source NGC 4051 (Hunt et al. 1992).

4.3 The Response of the High-Ionization Lines

The high-ionization emission lines in NGC 5548 have such short lags that their response was either unresolved (e.g., He II λ1640 and N V λ1240) or only marginally resolved (e.g., Lyα and C IV) with the four-day sampling of the original AGN Watch *IUE* study. Higher temporal resolution studies of these lines are highly desirable in at least two contexts. First, as discussed in Sec. 3.4, whether or not the transfer functions for Lyα and C IV have peaks at zero or displaced from zero can provide important information about the physics of the BLR clouds and possibly the geometry of the region. Second, the variability of the highest ionization lines, such as He II, implies that there are ionization fronts in gas within a few light days of the central source. Interaction with this gas might not only significantly modify the high-energy ionizing continuum before it reaches the C IV/Lyα zone (perhaps accounting for the high-energy depletion alluded to in Sec. 3.5), but the absorbing gas may also produce significant UV/optical continuum radiation and thus serve as the continuum reprocessing agent (Sec. 4.1). This would also provide a natural explanation for the similarity of the UV/optical continuum and emission-line variability time scales.

4.4 Two-Dimensional Transfer Functions and the Velocity Field of the BLR

Thus far in this discussion we have not made use of the fact that the radial-velocity structure of emission lines is resolved. Instead of examining only the integrated response of an emission line to continuum variations, we can measure the response as a function of radial velocity, and thus determine the velocity field of the BLR as well as its geometry (Blandford and McKee 1982; Capriotti et al. 1982; Robinson et al. 1990; Pérez et al. 1992a). The bulk velocity field can be determined simply by comparing the response of the line wings (i.e., high radial velocity) with the line core (low radial velocity) or shortward ("blue") line wing with the longward ("red") line wing. For example, if the velocity field is dominated by radial outflow, then the blue side of the emission line, which arises from the outflowing gas on the near side of the continuum source, will respond before the red side, which arises on the far side of the BLR. Similarly, if the BLR velocity field is characterized by rotation, either organized or random, the line wings will vary before the core and the variations will be symmetric about line center.

The formalism of Sec. 2 can be generalized to consider the line response as a function of radial velocity v as

$$L(v,t)=\int_{-\infty}^{\infty}\Psi(v,\tau)C(t-\tau)d\tau, \qquad (19)$$

which is called the "two-dimensional transfer equation." The two-dimensional, or velocity-dependent, transfer function $\Psi(v,\tau)$ is most easily shown as a contour plot or gray scale in v, τ space. Examples of such "echo images," from Welsh and Horne (1991), are shown in Fig. 8 for several different velocity fields (additional examples are shown by Pérez et al. 1992b). In these diagrams, the time-delay axis runs vertically, so at an arbitrary point on the horizontal axis we see the transfer function at a fixed radial velocity running vertically. The integrated response of the line $\Psi(\tau)$ [Eq. (9)] can be computed by summing the response at all velocities; this is shown to the right of each echo image. Similarly, the response of the line profile can be seen by integrating along the time delay axis, and this is shown underneath each echo image; the line profile shown is the difference profile obtained by subtracting the line profile observed at $\tau\leqslant 0$ from that observed at $\tau\geqslant\tau_{\max}$ for a step-function increase in the continuum level at $\tau=0$. The specific examples shown in Fig. 8 were selected because of the similarity of their one-dimensional transfer functions. With real data, it would be very difficult to distinguish among these possibilities only by solution for $\Psi(\tau)$. This demonstrates the importance of utilizing *all* of the information available from the spectra.

Two-dimensional transfer functions, as shown in Fig. 8, have not yet been published for any source. In the case of the *IUE* spectra of NGC 5548, the combination of the

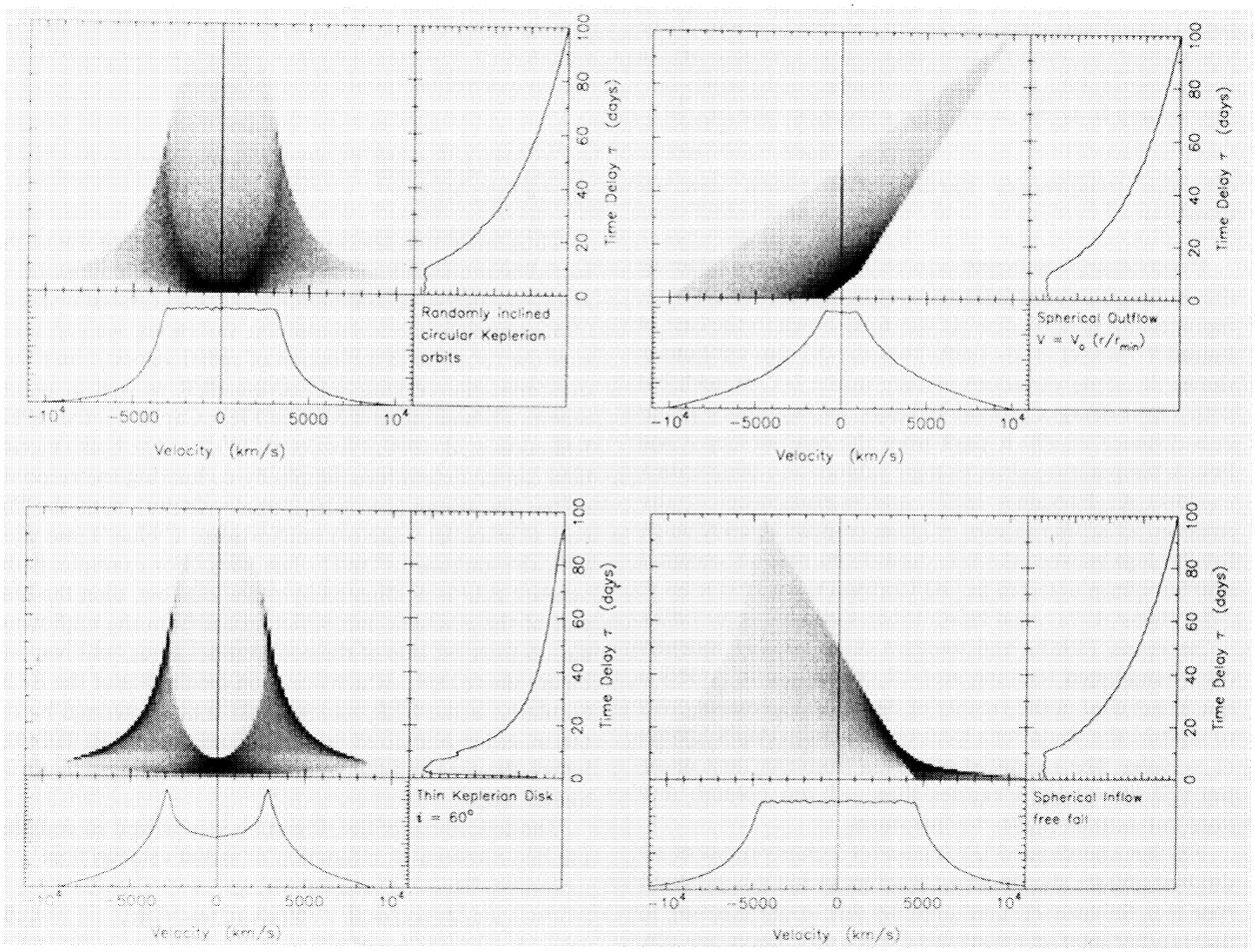

FIG. 8—Examples of two-dimensional echo images, from Welsh and Horne (1991), for various BLR geometries and velocity fields. The upper left panel of each image shows the two-dimensional transfer function as a gray-scale image in the velocity-time-delay plane. The one-dimensional transfer function $\Psi(\tau)$ is obtained by integrating over velocity, and this is shown in the upper right panel of each image. The line responsivity profile is obtained by integrating over time delay, and this is shown in the lower panel for each image. Despite having radically different geometries and/or velocity fields, the four examples shown here have very similar one-dimensional transfer functions; the two-dimensional transfer function would be required to distinguish among these possible models. Figure courtesy of W. F. Welsh.

limited signal-to-noise ratio and the short lags (relative to the sampling interval) are limiting factors. In the case of the AGN Watch optical data, the kind of analysis that can be performed is limited by the inhomogeneity of the database.

Some simpler analyses have been undertaken either by binning the data over large ranges in radial velocity or by examining changes in the line profiles. The results of these experiments have been somewhat mixed. In the case of NGC 5548, Clavel (1991) has cross-correlated the flux in the core (i.e., $|v| < 3000$ km s^{-1}) of the C IV line with the flux in the wings (i.e., $|v| > 3000$ km s^{-1}) and finds that the variations in the core follow those in the wings by 2 ± 2 days. This indicates the existence of a radial-velocity gradient in the BLR, and is suggestive of virial motion of some sort (either organized rotation or turbulence). Crenshaw and Blackwell (1990) reach a different conclusion by examination of the C IV profile evolution during the rapid decay of the third event; the red wing of C IV was observed to respond to the continuum decrease more rapidly than the blue wing. This indicates that the redshifted gas is closer to the line of sight, and thus argues for net *infall* of the BLR cloud system. Higher temporal resolution and higher signal-to-noise ratio data will probably be required to determine which, if either, of these results is correct. In the case of NGC 4151, Maoz et al. (1991) find no significant time lag between the variations of the red and blue wings of the Balmer lines, thus arguing against any net radial motion in this object. The C IV line shows compelling evidence for a radial-velocity gradient, similar to that detected in NGC 5548 (Clavel et al. 1990). In the case of Fairall 9, Koratkar and Gaskell (1989) conclude from cross-correlation of the red and blue wings of the C IV emission line that infall is the most probable velocity field for the BLR in this system.

It is worth commenting that in no case does *outflow* appear to be the most likely velocity field. This is potentially of profound importance, as it indicates that gravitation controls the dynamics of the BLR clouds. If indeed the BLR cloud system is gravitationally bound to the cen-

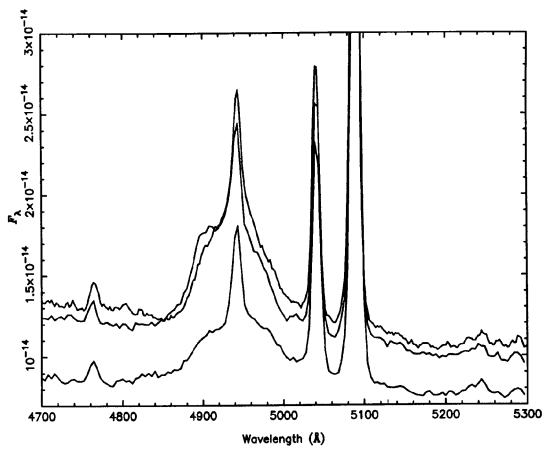

FIG. 9—Three spectra of NGC 5548 with different Hβ profiles. These spectra were obtained with the Ohio State CCD spectrograph on UT 1989 Mar 21=JD2447606 (middle), UT 1990 Dec 27=JD 2448252 (highest, with blueward asymmetry), and UT 1992 Sep 4=JD 2448869 (lowest, with redward asymmetry).

tral object, the virial theorem allows us to calculate the mass of the central source in NGC 5548 from the line-of-sight velocity dispersion of the BLR clouds ($v_{\rm FWHM}\approx 4500$ km s^{-1} for C IV) and the radius of the system (~ 10 lt days for C IV),

$$M\approx\frac{rv_{\rm FWHM}^2}{2G}\approx 2\times 10^7 M_\odot. \qquad (20)$$

The reader is cautioned that this is only an order of magnitude estimate since the relationship between v and r, which determines the numerical coefficient in this equation, is not known.

An alternative approach to direct solution of Eq. (19) is to assume a BLR geometry and velocity field, and use the line profiles to give the BLR emissivity distribution. It is then straightforward to compute the one-dimensional transfer function $\Psi(\tau)$ for this model and compare it with the experimental result (Mannucci et al. 1992).

4.5 Evolution of the BLR Structure

While the evidence for line-profile variations on the BLR light-travel time scale is somewhat ambiguous, there is clear evidence for very pronounced profile variations on longer time scales, as shown in Fig. 9. If profile variability were solely attributable to the presence of excitation inhomogeneities in the BLR (Capriotti et al. 1982), then the line structure would change on time scales shorter than $\sim r/c$; however, the observed time scales for profile variability tend to be more like the dynamical time scales [Eq. (8)] than light-travel time scales, which suggests but does not prove that the profile changes are due to real changes in the BLR gas distribution. No clear patterns have emerged from the rather limited profile variability studies which have been undertaken to date, and indeed the variations appear to be quite complex. The line profiles in NGC 5548 appear to have variable components both blueward and redward of line center, and their variations do not appear to be correlated with one another or with the continuum state (e.g., see Stirpe et al. 1988; Peterson et al. 1990; Stirpe and de Bruyn 1991). Other AGNs with complex profile behavior include Akn 120 (Korista 1992, and references therein), which seems to show as many as four individual features at different radial velocities that come and go in no deciphered pattern, and 3C 390.3 (Veilleux and Zheng 1991), whose highly structured line profiles Zheng et al. (1991) have attempted to describe with a double-stream BLR model, or a rotating disk with a region of enhanced brightness. Unfortunately, no high sampling-rate (relative to the light-travel time) monitoring programs have yet been carried out over even a few times $\tau_{\rm dyn}$ for any source. Such programs will be necessary to determine conclusively whether there is any pattern to profile variations, or if they are more or less random events, perhaps associated with instabilities in the BLR gas.

It is worth mentioning in passing that a small number of AGNs appear to have emission-line profiles that can be fitted well with relativistic disk models (e.g., Chen et al. 1989; Halpern 1990). Lines which arise in an inclined Keplerian disk have a characteristic double-horn shape (cf. Fig. 8), and if the disk is rotating at relativistic velocities, the blue side of the line profile has a higher intensity than the red side because the radiation from the approaching side of the disk is Doppler-boosted. In principle, such a model can be tested with even limited profile variability data because this model predicts (a) that the red and blue sides of the profiles should vary in phase, and (b) that the intensity of the blue side should always exceed that of the red side. Miller and Peterson (1990) have shown a spectrum of Arp 102B in which neither of these conditions appears to be met, thus casting some doubt on applicability of simple, axisymmetric relativistic disk models of the BLR.

4.6 Nonlinear Emission-Line Response

The issue of whether or not the emission lines respond to continuum variations in a linear fashion has been mentioned earlier, in Secs. 2.2 and 3.5. There are several effects that might lead to nonlinear emission-line response, such as (1) nonvariable contributions to the emission lines and/or the continuum, (2) dilution of the line response by light-travel time effects in a physically thick BLR, (3) a change in shape of the ionizing continuum, and (4) nonlinear physical processes; it is the last of these which will be considered in this section. A simple example of this would be in a BLR cloud with complicated ionization structure. Suppose, e.g., that the most abundant carbon ion at the ionized face of a cloud is C^{+3}, but deeper into the cloud, the dominant ion becomes C^{+2}. It is conceivable that an increase in the ionizing flux could increase the size of the C^{+3} zone, leading to an enhancement of C IV λ1549 emission, and decrease the size of the C^{+2} zone, thus also leading to a net *decrease* in the strength of C III] λ1909. Another example is the case of collisionally excited lines, since these are sensitive to the temperature, which is a nonlinear

TABLE 3
BLR Radius-Luminosity Relationship

Galaxy	log L_λ	r (lt days)
(1)	(2)	(3)
UV observations:		
NGC 4151 [a]	38.8	4
NGC 5548 [b]	40.2	10
Akn 120 [c]	41.2	39::
Fairall 9 [d]	41.1	155
Optical observations:		
NGC 4151 [e]	38.7	9
NGC 5548 [f]	39.5	18
Mrk 279 [g]	39.8	12
Mrk 590 [h]	39.8	19

[a] Clavel et al. 1990
[b] Clavel et al. 1991
[c] Peterson & Gaskell 1991
[d] Clavel, Wamsteker, & Glass 1989
[e] Maoz et al. 1991
[f] Peterson et al. 1992
[g] Maoz et al. 1990
[h] Peterson et al. 1993

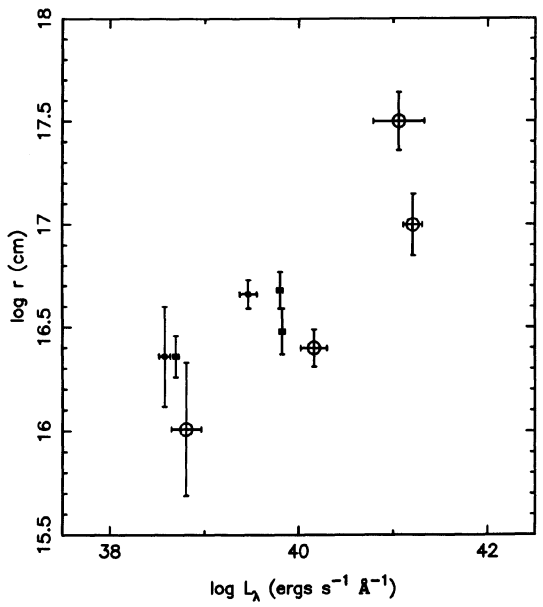

FIG. 10—BLR radius-luminosity relationship for the AGNs listed in Table 3, plotted on a scale where $r \propto L^{1/2}$ [Eq. (21)] gives a 45° line. The open circles are for UV data, and the filled circles are for optical data. The uncertainties in the BLR radius are as given in the original references. The specific luminosities (for $h_0=1$) are usually measured at about 1350 Å for the UV data and at about 5100 Å for the optical data. For the UV data, r is given by $c\tau_{\rm peak}$ for C IV, and for the optical data, r is given by $c\tau_{\rm peak}$ for Hβ (or Hα in the case of Mrk 279). The error bars in luminosity reflect the rms variation in L_λ during the period that r was measured.

function of the ionizing flux. Recombination lines, on the other hand, can usually be expected to vary in a way that is close to linear, unless non-nebular conditions obtain. In particular, in an optically thick, pure hydrogen nebula, the number of Lyα photons should equal the number of ionizing photons.[5] Departures from this occur if there are Lyα destruction mechanisms. Under the BLR conditions in NGC 5548, Shields and Ferland (1993) show that the Lyα production rate decreases with increasing continuum flux. This occurs on account of (1) increased destruction of Lyα by Balmer continuum absorption, (2) the increased population of the $n=2$ state, which can result in additional ionization of H by lower-energy photons rather than inevitable production of Lyα photons, and (3) line thermalization from the increased rate of collisional excitation. Taking these effects into account, it is possible to explain the observed value $\gamma \approx 0.5$–0.6 [Eq. (18)] for Lyα (Krolik et al. 1991; Pogge and Peterson 1992).

For other lines, it is indeed possible that the responsivity could actually *decrease* with an increasing continuum flux, and this may be another way to account for a deficit of line response near $\tau=0$. This has been suggested by Sparke (1993), who argues that the narrowness of the line autocorrelation functions compared to the continuum autocorrelation function can be interpreted as an indication of negative responsivity. Current implementations of the MEM technique used to solve Eq. (11) have not dealt with this possibility.

Another approach, also originally suggested by Blandford and McKee (1982), is model-fitting. For a particular BLR geometry, the degree of emission-line anisotropy, the radial emissivity (or responsivity) distribution, velocity field, etc., are free parameters that can be determined by a multidimensional fit to the emission-line light curves. O'Brien and Goad (1993) have attempted this with the Lyα and Mg II light curves for NGC 5548, and find that anisotropic, nonlinear models for the line emission fit the data much better than linear, isotropic models.

4.7 The Generality of the NGC 5548 Results

Well-sampled, high-quality data such as those obtained for NGC 5548 are needed for other AGNs in order to test the generality of the AGN Watch results. It would be especially interesting to compare the NGC 5548 results with those obtained from a study of AGNs with markedly different line-profile characteristics (i.e., line-of-sight velocity fields). This may clear up some ambiguities that might arise from viewing individual systems at different inclinations, and may provide us with new insights into the types of detailed *structure* that we observe in the broad-line profiles and how and why this structure changes with time. An excellent candidate is the broad-line radio galaxy 3C 390.3, which has very complex, variable emission-line profiles (Veilleux and Zheng 1991).

It is also important to examine AGNs over as wide a range in luminosity as possible, as this can provide impor-

[5] That the number of Lyα photons emitted by an optically thick gas equals the number of ionizing photons absorbed by the gas can be used to determine the "covering factor" for the BLR, i.e., the fraction of the sky covered by BLR clouds as seen by the central source. For NGC 5548, the mean broad-line Lyα luminosity is $L(\text{Ly}\alpha) \approx 1.8\times10^{42} h_0^{-2}$ ergs s^{-1}. The number of Lyα photons emitted per second is thus $N(\text{Ly}\alpha) = L(\text{Ly}\alpha)/h\nu_\alpha \approx 1.1\times10^{53} h_0^{-2}$ s^{-1}, where $h\nu_\alpha$ is the energy per Lyα photon. The covering factor f is given by the fraction of all ionizing photons, $Q(H)$ in Eq. (17), that are absorbed by the BLR clouds, i.e., $f = N(\text{Ly}\alpha)/Q(H) \approx 0.1$. This value of the covering factor was used at the beginning of Sec. 2.1.

tant information about the general characteristics of the AGN phenomenon. We can consider, e.g., how the BLR size scales with luminosity. Since the luminosity L of the central source is proportional to the rate at which it produces ionizing photons, by Eq. (17),

$$r \propto L^{1/2}. \tag{21}$$

In order to test how well this apparently simple prediction holds up, all published measurements of lags which are "reasonably" well determined have been collected in Table 3. For the ultraviolet data, the continuum luminosity given is the specific luminosity (ergs s^{-1} $Å^{-1}$) at about 1350 Å in the rest frame of the source, and the BLR radius is taken to be $r=c\tau_{\rm peak}$, where $\tau_{\rm peak}$ is the lag for C IV. For the optical data, the specific luminosity is measured around 5100 Å, and $\tau_{\rm peak}$ is for either Hβ or Hα. These data are also plotted in Fig. 10, which shows that, allowing for the very few data points available, the agreement with the prediction of Eq. (21) is not too bad for either the ultraviolet or the optical data.[6] A similar result has been published by Koratkar and Gaskell (1991b), based on less well-determined lag measurements.

The apparent consistency between the data and the predicted radius-luminosity relation is especially striking when one considers the implicit assumptions underlying Eq. (21), namely (1) that the continuum shape does not vary greatly with luminosity or from object to object, (2) that the BLR is characterized by the same values of the parameters U and n_H, regardless of luminosity, and (3) that the lag is a reliable measure of r/c. We certainly know that none of these assumptions is very good at some level; indeed, it was noted in Sec. 3.4 that both simulations (e.g., Robinson and Pérez 1990) and real data show that the lag can vary by a factor of a few or more depending on the characteristics of the continuum variations.

For a number of reasons, it is important to increase the number of galaxies for which consistency with Eq. (21) can be tested. As pointed out by Dibai (1981) and in numerous subsequent papers (see references in Koratkar and Gaskell 1991b), if the BLR cloud system is virialized, one can combine Eqs. (21) and (20) to obtain a mass-luminosity relationship for AGNs. Also, if it were shown that a single radius-luminosity relationship is valid over a large range in luminosity, it would be a strong indication that similar physical processes are at work in both high- and low-luminosity AGNs.

Since there are few nearby AGNs with luminosities much lower than those already observed, extending the luminosity range over which Eq. (21) can be tested requires intensive monitoring programs on high-luminosity AGNs (quasars). For a variety of reasons, these have not been carried out. First, suitable candidates tend to be apparently faint. The AGN luminosity function is quite steep, so high-luminosity AGNs are relatively rare per unit volume, and thus when they are found they tend to be at large distances. To obtain the data quality required for reverberation mapping, a large telescope is required. Second, if indeed Eq. (21) is valid, then the time scales for emission-line variability are longer in more luminous objects, and monitoring campaigns of longer duration are required. Third, distant objects are highly redshifted. This has two detrimental effects: First, the rest-frame ultraviolet, which is observable from the ground at high redshift, has no suitably strong narrow lines for internal calibration of ground-based spectra (cf. Sec. 2.4), and the rest-frame optical becomes shifted into the hard-to-observe infrared. Second, time-dilation further lengthens the variability time scale by a factor of $1+z$. Finally, high-luminosity AGNs seem to undergo lower-amplitude variations than low-luminosity AGNs (e.g., Edelson et al. 1990), thus decreasing the probability of a successful outcome of a monitoring program. Indeed, LAG monitoring two quasars for five months during 1990, but detected no emission-line variability and little continuum variability in either case (Jackson et al. 1992). Certainly, there are many recent reports of detection of short time-scale emission-line variability in high-luminosity sources (e.g., Gondhalekar et al. 1986; Zheng et al. 1987; O'Brien et al. 1989; Pérez et al. 1989; Gondhalekar 1990; Sitko 1990; Koratkar and Gaskell 1991a; Korista 1991; O'Brien and Harries 1991), but the fraction of sources in which emission-line variability is detected seems to be smaller for QSOs than for Seyfert galaxies (e.g., Peterson et al. 1985; Edelson et al. 1990; Rosenblatt et al. 1992). Moreover, in the case of at least some of the most luminous sources, anisotropic continuum emission may complicate things; the high polarization and rapid continuum variability of some of these sources are thought to be attributable to beamed radiation. Thus, while programs on high-luminosity sources are extremely desirable, they will be relatively difficult to carry out in practice.

As a cautionary note, it may well be that the existing data are not very representative AGNs as a class, and that subtle, unidentified selection effects are operating. All of the galaxies for which lag measurements exist are by necessity highly variable sources. The successful monitoring programs that have been undertaken to data have targeted specific AGNs that were known *a priori* to vary with fairly large amplitudes on appropriate time scales. With the exception of Fairall 9, which varied by a factor of $\sim$30 over a few years, the AGNs listed in Table 3 show continuum variations of about a factor of a few (maximum to minimum flux) over the course of a single observing season. By selecting such galaxies as targets for monitoring programs, we enhance the probability of successfully obtaining a measurement of the lag, but we may be selecting AGNs with very special intrinsic characteristics, or which are viewed at some preferred aspect.

4.8 Future Programs

At least some of the questions concerning the generality of the NGC 5548 results are likely to be addressed in the near future on the basis of data from monitoring programs that have been recently completed or are currently under way. At the time of writing, the International AGN Watch

[6]Recall that these relationships have different zero points because they are referenced to different continuum bands and to different emission lines.

has just completed a second comprehensive study, on the southern hemisphere Seyfert 1 galaxy NGC 3783, and the first results of the *IUE* and ground-based programs should be ready soon. Members of LAG have presented a number of preliminary reports at conferences, and several papers describing their results are also forthcoming. These data will allow more critical tests of the radius-luminosity relationship [Eq. (21)] and provide important information about the transfer function in sources of different mean luminosity and different line-of-sight velocity fields.

Some of the more challenging questions mentioned in this section have to do with emission-line response on very short time scales (e.g., the amplitude of transfer functions at zero delay and the lag for the highest ionization lines). Higher temporal sampling than has been achieved already will be required to address these questions. The issue of whether or not there is an ordered velocity field in the BLR of NGC 5548 and other sources is still open— resolution of this question will also require a shorter interval between observations, since the four-day interval between observations in the 1988–1989 campaign is about half the measured lag for the strongest emission lines, Lyα and C IV, and this is insufficient to detect short time-scale profile changes. A search for velocity-dependent line response will require not only a finer temporal grid of observations, but also higher signal-to-noise ratio data than can be obtained with *IUE*. In order to address these important questions with high-quality, well-sampled data, the International AGN Watch is carrying out a limited-duration high-intensity campaign involving both *Hubble Space Telescope* and *IUE*. This campaign is tentatively scheduled for the spring of 1993, and will be complemented by the continuing ground-based observations of this object, which are now moving into a fifth year.

Long-term monitoring programs, such as the ground-based effort on NGC 5548 and the EEC *IUE*-based program on NGC 4151, are an area of special importance. The BLR can be expected to undergo changes in geometry on time scales of order τ_{dyn} [Eq. (8)]. Intensive spectroscopic monitoring on time scales several times this long should be able to reveal the processes that cause line-profile variations and should show whether or not there are bulk motions of gas clouds that are related to the process by which AGNs are fueled.

A more formidable observational problem is to determine the relationship between the X-ray spectrum and the lower-energy continuum. The practical difficulty is obtaining sufficient X-ray observations, since both high- and low-temporal frequencies need to be well sampled. The biggest problem is that there are very few X-ray data on time scales most relevant for UV/optical continuum variability (days to weeks), and such data will almost certainly be required to establish observationally the causal relationship between the X-ray and UV/optical continua.

5. CONCLUSIONS

The relationship between continuum and broad emission-line variability provides a unique probe of the central regions of AGNs, and allows us to extract information about the shape and nature of the unobservable extreme ultraviolet continuum and the geometry and kinematics of the BLR that cannot be obtained through any direct method. Reverberation mapping of the BLR essentially provides spatial resolution corresponding to microarcsecond projected scales for nearby AGNs.

While the principles of reverberation mapping have been understood for some time, it has been only within the last few years that the massive databases required for successful applications of this technique have been assembled. The results obtained by the International AGN Watch on the Seyfert galaxy NGC 5548 have been discussed in some detail to illustrate the wealth of information that can be obtained. Already several important conclusions have been reached: the UV and optical continua are found to vary together with no detectable phase difference, the variable parts of the strong, broad emission lines are found to arise much closer to the central source than previously supposed, and the line-emitting region shows strong evidence of radial ionization stratification. Each of these has important physical consequences. A number of important new questions have emerged, and new, more sophisticated questions are being asked about the nature of the AGN continuum and the BLR. There is no doubt that reverberation mapping results are fundamentally changing our views about the inner regions of AGNs, and that the future of this technique holds great promise for continued advances.

I wish to thank D. Alloin, J. Clavel, K. Horne, D. Maoz, R. W. Pogge, J. C. Shields, and G. M. Stirpe for valuable criticisms and comments on an earlier draft of this review. I am pleased to acknowledge support for emission-line variability and reverberation mapping studies at The Ohio State University by the National Science Foundation through Grant No. AST-9117086 and by NASA through a Long-Term Space Astrophysics grant. I also wish to thank J. E. Hesser for suggesting this review.

REFERENCES

Antokhin, I. I., and Bochkarev, N. G. 1983, Soviet Astron., 27, 261
Bahcall, J. N., Kozlovsky, B.-Z., and Salpeter, E. E. 1972, ApJ, 171, 467
Baldwin, J. A. 1977, ApJ, 214, 679
Baribaud, T., and Alloin D. 1990, A&A, 236, 346
Baribaud, T., Alloin D., Glass, I., and Pelat, D. 1992, A&A, 256, 375
Barvainis, R. 1987, ApJ, 320, 537
Binette, L., Prieto, A., Szuszkiewicz, E., and Zheng, W. 1989, ApJ, 343, 135
Binette, L., and Raga, A. C. 1990 AJ, 100, 1046
Blandford, R. D. 1992, in Relationships Between Active Galactic Nuclei and Starburst Galaxies, ed. A. V. Filippenko (San Francisco, Astronomical Society of the Pacific), p. 455
Blandford, R. D., and McKee, C. F. 1982 ApJ, 255, 419
Blandford, R. D., Netzer, H., and Woltjer, L. 1990, Active Galactic Nuclei, Saas-Fee Advanced Course 20, ed. T. J. -L. Courvoisier and M. Mayor (Berlin, Springer)

Capriotti, E. R., Foltz, C. B., and Peterson, B. M. 1982 ApJ, 261, 35
Chen, K., Halpern, J. P., and Filippenko, A. V. 1989, ApJ, 339, 742
Clavel, J. 1991, in Variability of Active Galactic Nuclei, ed. H. R. Miller and P. J. Wiita (Cambridge, Cambridge University Press), p. 301
Clavel, J., et al. 1991, ApJ, 366, 64
Clavel, J. 1990, MNRAS, 246, 668
Clavel, J., et al. 1992, ApJ, 393, 113
Clavel, J., and Santos-Lleó, M. 1990, A&A, 230, 3
Clavel, J., Wamsteker, W., and Glass, I. S. 1989, ApJ, 337, 236
Collin-Souffrin, S. 1991, A&A, 249, 344
Collin-Souffrin, S., Joly, M., Dumont, S., and Pequignot, D. 1986, A&A, 166, 27
Coudrec, P. 1939, Ann. d'Astrophys., 2, 271
Courvoisier, T. J.-L. 1991, in Variability of Active Galaxies, ed. W. J. Duschl, S. J. Wagner, and M. Camenzind (Berlin, Springer), p. 214
Courvoisier, T. J.-L., and Clavel, J. 1991, A&A, 248, 389
Crenshaw, D. M., and Blackwell, J. H., Jr. 1990, ApJ, 358, L37
Dibai, E. A. 1981, Soviet Astron., 28, 245
Dietrich, M., et al. 1993, ApJ, 408, in press.
Done, C., et al. 1990, MNRAS, 243, 713
Edelson, R. A., and Krolik, J. H. 1988, ApJ, 333, 646
Edelson, R. A., Krolik, J. H., and Pike, J. F. 1990, ApJ, 359, 86
Elvis, M., et al. 1986, ApJ, 310, 291
Emmering, R. T., Blandford, R. D., and Shlosman, I. 1992, ApJ, 385, 460
Fabrika, S. N. 1980a, Soviet Astron. Lett., 6, 293
Fabrika, S. N. 1980b, Soviet Tsirk., No. 1109
Ferland, G. J., Korista, K. T., and Peterson, B. M. 1990 ApJ, 363, L21
Ferland, G. J., and Mushotzky, R. F. 1982 ApJ, 262, 564
Ferland, G. J., and Netzer, H. 1979, ApJ, 229, 274
Ferland, G. J., Netzer, H., and Shields, G. A. 1979, ApJ, 232, 382
Ferland, G. J., Peterson, B. M., Horne, K., Welsh, W. F., and Nahar, S. N. 1992, ApJ, 387, 95
Gaskell, C. M., and Peterson, B. M. 1987, ApJ, 65, 1
Gaskell, C. M., and Sparke, L. S. 1986, ApJ, 305, 175
Glass, I. S. 1992, MNRAS, 256, 23P
Goad, M. R., O'Brien, P. T., and Gondhalekar, P. M. 1993, MNRAS, in press
Gondhalekar, P. M. 1990, MNRAS, 243, 443
Gondhalekar, P. M. 1992, MNRAS, 255, 663
Gondhalekar, P. M., O'Brien, P. T., and Wilson, R. 1986, MNRAS, 222, 71
Halpern, J. P. 1990, ApJ, 365, L51
Horne, K. 1993, in preparation
Horne, K., Welsh, W. F., and Peterson, B. M. 1991, ApJ, 367, L5
Hummer, D. G., and Kunasz, P. B. 1980, ApJ, 236, 609
Hunt, L. K., Mannucci, F., Salvati, M., and Stanga, R. M. 1992, A&A, 257, 434
Jackson, N., et al. 1992, A&A, 262, 17
Kaastra, J. S., and Barr, P. 1989, A&A, 226, 59
Kazanas, D. 1989, ApJ, 347, 74
Kinney, A. L., Rivolo, A. R., and Koratkar, A. P. 1990, ApJ, 357, 338
Kondo, Y., ed., 1987, Exploring the Universe with the IUE Satellite (Dordrecht, Reidel)
Koratkar, A. P., and Gaskell, C. M. 1989, ApJ, 345, 637
Koratkar, A. P., and Gaskell, C. M. 1991a, ApJS, 75, 719
Koratkar, A. P., and Gaskell, C. M. 1991b, ApJ, 370, L61
Koratkar, A. P., and MacAlpine, G. M. 1992, ApJ, 401, 110
Korista, K. T. 1991, AJ, 102, 41
Korista, K. T. 1991, ApJS, 79, 285
Krolik, J. H., Horne, K., Kallman, T. R., Malkan, M. A., Edelson, R. A., and Kriss, G. A. 1991, ApJ, 371, 541
Kwan, J., and Krolik, J. H. 1981, ApJ, 250, 478
Laor, A., and Netzer, H. 1989, MNRAS, 238, 897
Lynden-Bell, D., and Pringle, J. 1974, MNRAS, 168, 603
Malkan, M. A., and Sargent, W. L. W. 1982, ApJ, 254, 122
Mannucci, F., Salvati, M., and Stanga, R. M. 1992, ApJ, 394, 98
Maoz, D. 1992, in Physics of Active Galactic Nuclei, ed., W. J. Duschl and S. J. Wagner (Berlin, Springer), p. 214
Maoz, D., and Netzer, H. 1989, MNRAS, 236, 21
Maoz, D., et al. 1991, ApJ, 367, 493
Maoz, D., et al. 1990, ApJ, 351, 75
Maoz, D., et al. 1993, ApJ, 404, in press
Maraschi, L., et al. 1991, ApJ, 368, 138
Mathews, W. G., and Ferland, G. J. 1987, ApJ, 323, 456
McHardy, I. 1988, Mem. Soc. Astron. Ital., 59, 239
Miller, J. S., and Peterson, B. M. 1990, ApJ, 361, 98
Molendi, S., Maraschi, L., and Stella, L. 1991, in Variability of Active Galaxies, ed. W. J. Duschl, S. J. Wagner, and M. Camenzind (Berlin, Springer), p. 65
Morini, M., et al. 1986, ApJ, 307, 486
Nandra, K., Pounds, K. A., Stewart, G. C., George, I. M., Hayashida, K., Makino, F., and Ohasi, T. 1991, MNRAS, 248, 760
Netzer, H. 1989, Comm. Astrophys., 89, 137
Netzer, H. 1991, in Variability of Active Galaxies, ed. W. J. Duschl, S. J. Wagner, and M. Camenzind (Berlin, Springer), p. 107
Netzer, H., and Maoz, D. 1990, ApJ, 365, L5
Netzer, H., et al. 1990, ApJ, 353, 108
O'Brien, P. T., and Goad, M. R. 1993, preprint
O'Brien, P. T., and Harries, T. J. 1991, MNRAS, 250, 133
O'Brien, P. T., Zheng, W., and Wilson, R. 1989, MNRAS, 233, 845
Osterbrock, D. E. 1989, Astrophysics of Gaseous Nebulae and Active Galactic Nuclei (Mill Valley, University Science Books)
Osterbrock, D. E. 1991, Rep. Progr. Phys., 54, 579
Osterbrock, D. E. 1993, ApJ, in press
Penston, M. V. 1988, MNRAS, 233, 601
Penston, M. V. 1991, in Variability of Active Galactic Nuclei, ed. H. R. Miller and P. J. Wiita (Cambridge, Cambridge University Press), p. 343
Pérez, E. Penston, M. V., and Moles, M. 1989, MNRAS, 239, 75
Pérez, E., Robinson, A., and de la Fuente, L. 1992a, MNRAS, 255, 502
Pérez, E., Robinson, A., and de la Fuente, L. 1992b, MNRAS, 256, 103
Perola, G. C., et al. 1986, ApJ, 306, 508
Peterson, B. M. 1988, PASP, 100, 18
Peterson, B. M. 1991, in Variability of Active Galaxies, ed. W. J. Duschl, S. J. Wagner, and M. Camenzind (Berlin, Springer), p. 47
Peterson, B. M. 1992, in Relationships Between Active Galactic Nuclei and Starburst Galaxies, ed. A. V. Filippenko (San Francisco, Astronomical Society of the Pacific), p. 29
Peterson, B. M., et al. 1991, ApJ, 368, 119
Peterson, B. M., et al. 1991, ApJ, 392, 470
Peterson, B. M., Ali, B., Horne, K., Bertram, R., Lame, N. J., Pogge, R. W., and Wagner, R. M. 1993, ApJ, 402, 469
Peterson, B. M., Crenshaw, D. M., and Meyers, K. A. 1985, ApJ, 298, 283

Peterson, B. M., and Gaskell, C. M. 1991, ApJ, 386, 152
Peterson, B. M., Meyers, K. A., Capriotti, E. R., Foltz, C. B., Wilkes, B. J., and Miller, H. R. 1985, ApJ, 292, 164
Peterson, B. M., Reichert, G. A., Korista, K. T., and Wagner, R. M. 1990, ApJ, 352, 68
Pogge, R. W., and Peterson, B. M. 1992, AJ, 103, 1084
Rees, M. J. 1984, ARA&A, 22, 471
Rees, M. J., Netzer, H., and Ferland, G. J. 1989, ApJ, 347, 640
Reichert, G. A., et al. 1991, in Variability of Active Galactic Nuclei, ed. H. R. Miller, and P. J. Wiita (Cambridge, Cambridge University Press), p. 335
Robinson, A., and Pérez, E. 1990, MNRAS, 244, 138
Robinson, A., Pérez, E., and Binette, L. 1990, MNRAS, 246, 349
Rodríguez-Pascual, P. M., Santos-Lleó, M., and Clavel, J. 1989, A&A, 219, 101
Rokaki, E., and Magnan, C. 1992, A&A, 261, 41
Romanishin, W., et al. 1993, in preparation
Rosenblatt, E. I., Malkan, M. A., Sargent, W. L. W., and Readhead, A. C. S. 1992, ApJS, 81, 59
Sanders, D. Phinney, E. S., Neugebauer, G., Soifer, B. T., and Matthews, K. 1989, ApJ, 347, 29
Schaaf, R., and Schmutzler, T. 1992, in Physics of Active Galactic Nuclei, ed. W. J. Duschl and S. J. Wagner (Berlin, Springer), p. 230
Scoville, N., and Norman, C. 1988, ApJ, 332, 163
Shakura, R. I., and Sunyaev, R. A. 1973, A&A, 24, 337
Shields, J. C., and Ferland, G. J. 1993, ApJ, 402, 425
Sitko, M. L. 1990, ApJS, 72, 777
Sitko, M. L. 1991, in Variability of Active Galactic Nuclei, ed., H. Miller and P. J. Wiita (Cambridge, Cambridge University Press), p. 104
Sparke, L. S. 1993, ApJ, in press
Stirpe, G. M., and de Bruyn, A. G. 1991, A&A, 245, 355
Sitrpe, G. M., de Bruyn, A. G., and van Groningen, E. 1988, A&A, 200, 9
Terlevich, R. 1992, in Relationships Between Active Galactic Nuclei and Starburst Galaxies, ed. A. V. Filippenko (San Francisco, Astronomical Society of the Pacific), p. 133
Terrell, J. 1967, ApJ, 147, 827
Ulrich, M.-H., et al. 1984, MNRAS, 206, 221
Ulrich, M.-H., et al. 1991, ApJ, 382, 483
van Groningen, E., and Wanders, I. 1992, PASP, 104, 700
Veilleux, S., and Zheng, W. 1991, ApJ, 377, 89
Voit, G. M., and Shull, J. M. 1988, ApJ, 331, 197
Walter, R., and Courvoisier, T. J.-L. 1991, A&A, 250, 312
Wamsteker, W., et al. 1990, ApJ, 354, 446
Wanders, I., et al. 1993, in preparation
Wanders, I., Peterson, B. M., Pogge, R. W., DeRobertis, M. M., and van Groningen, E. 1992, A&A, 266, 72
Welsh, W. F., and Horne, K. 1991, ApJ, 379, 586
Wills, B. J., Netzer, H., and Wills, D. 1985, ApJ, 288, 94
Woltjer, L. 1959, ApJ, 130, 38
Zeldovich, Y. B., and Novikov, I. D. 1964, Dokl. Akad. Nauk. SSSR, 158, 881
Zheng, W. 1991, ApJ, 382, L55
Zheng, W., Burbidge, E. M., Smith, H. E., Cohen, R. D., and Bradley, S. E. 1987, ApJ, 322, 164
Zheng, W., Veilleux, S., and Grandi, S. A. 1991, ApJ, 381, 418